Author:
Tipping, Hannah E

Title:
Experimental investigations into immersive ice nucleation

Experimental investigations into immersive ice nucleation

By

HANNAH TIPPING

Department of Physics
UNIVERSITY OF BRISTOL

A dissertation submitted to the University of Bristol in accordance with the requirements of the degree of MASTERS BY RESEARCH in the Faculty of Science.

SEPTEMBER 2022

Word count: c.14570

ABSTRACT

Ice nucleation has a significant role in many fields of research, with many questions of its behaviour still unanswered. The purpose of this thesis was to investigate three different aspects of immersive ice nucleation. These included the development of a cold stage that could be used with microfluidics, an investigation into the affects of salinity on the freezing temperature of snow and a determination on whether Homogentisate-1,2-dioxygenase (HGD) acts as an ice nucleator or an anti-freeze protein. These each pose important implications on areas such as climate change and cryopreservation. The cold stage or Automated Lag-Time Apparatus (ALTA) was successfully able to reach temperatures as low as -28.7°C with the use of a thermally conductive paste, making it a viable option for linear and isothermal experiments in the future. Further incorporating this with microfluidics will provide large sample sizes of small droplets giving statistically valuable data sets. The results from the British Antarctic Survey portrayed a minimal effect of salinity on the Arctic snow samples, with no signifcant freezing point depression observed. Where the freezing point increased due to INPs, it was most likely caused by biological particles such as ultramicrobacteria or exudates from phytoplankton. Finally, HGD was shown to act as an ice nucleator, increasing the freezing rate and causing the sample to freeze at a higher temperature. The HGD samples also experienced dendritic ice formation, causing a two step freezing pattern. Theories surrounding these results are discussed as well as suggestions for future experiments.

ACKNOWLEDGEMENTS

First of all I would like to thank Professor Walther Schwarzacher for his advice and support with this Masters and for helping me find the confidence to be independent in my research.

I am very grateful to the team at the British Antarctic Survey specifically Dr. Markus Frey, Dr. Amelie Kirchgaessner and Dr. Floortje Van Den Heuvel for allowing me to work in their Cambridge lab and to use the data I obtained. It was an amazing experience and I am very thankful for that opportunity.

I am also grateful to Professor Annela Seddon for her help in the materials lab and to Ellen Carrick for providing the HGD sample used in this research. I would also like to thank Sarah Alsalhi for patiently explaining techniques and equipment to me that were vital in this project.

Finally, I would like to thank my family as well as Karsten, Josh and Dimitra for their continued support and encouragement.

AUTHOR'S DECLARATION

I declare that the work in this dissertation was carried out in accordance with the requirements of the University's Regulations and Code of Practice for Research Degree Programmes and that it has not been submitted for any other academic award. Except where indicated by specific reference in the text, the work is the candidate's own work. Work done in collaboration with, or with the assistance of, others, is indicated as such. Any views expressed in the dissertation are those of the author.

SIGNED: ..... DATE: .....

TABLE OF CONTENTS

LIST OF TABLES

TABLE **Page**

LIST OF FIGURES

FIGURE **Page**

CHAPTER 1

INTRODUCTION

Nucleation is the first step in the creation of a crystal and represents a new thermodynamic phase [7]. It is relevant to any processes involving condensation, melting, freezing or evaporation making it significant to numerous areas of research. Recent developments in the understanding of ice nucleation have provided vital information on the production of drugs, natural gas hydrates and colloidal particles [8]. The area of focus during this study was the freezing phase transition in heterogeneous ice nucleation. This process is crucial to the development of cryopreservation [9] and to investigations into climate change as ice formation affects cloud properties [10] and sea ice [11].

Ice nucleation occurs in one of two ways: homogeneously or heterogeneously. Homogeneous nucleation is rarer, occuring randomly in time and space and without the presence of an ice nucleating particle to catalyze the phase transition [12]. Heterogeneous nucleation however is much more common, utilising the surfaces of impurities to help overcome the free energy barrier and achieve a phase transition [7]. There are three distinct modes of heterogeneous freezing: immersion, contact and deposition. As can be seen in figure 1.1, immersion freezing occurs when an ice nucleating particle (INP) is submerged within supercooled water, triggering the water to freeze around it. Contact freezing takes place when an INP is at the surface of a droplet and deposition freezing requires no prior condensation, as the water vapour freezes directly on contact with the INP [13]. Although all of these are commonly found, especially in cloud formation, only immersion freezing is relevant to the research conducted in this study, with contact freezing possible due only to potential contamination.

There are many kinds of INPs including mineral dusts (e.g. K-feldspars)[14], bioaerosols (e.g. bacteria, fungal spores, pollen) [15], crystalline salts (e.g. NaCl, KCl) [16] and pollutants (e.g. soot)[17]. Although all very different, there are a number of requirements for INPs to be effective ice nucleators. These were set out by Pruppacher and Klett as being: insolubility, a size large enough to support a critical nucleus, a crystallographic lattice match with ice and the ability to chemically bond with the

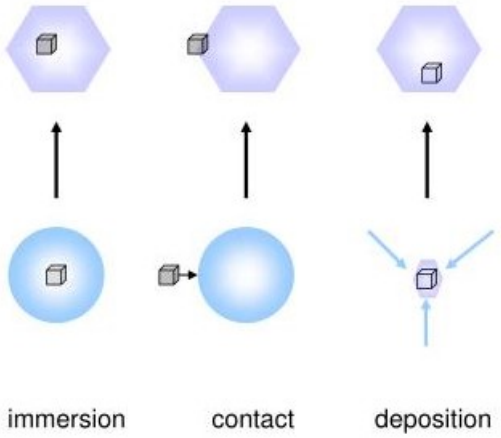

Figure 1.1: The three modes of heterogeneous ice nucleation. Taken from a presentation by Seifert *et al* [1]

surface of the ice [18]. Whilst these may be true for the majority of INPs there are exceptions to the rule, for example the ice nucleating ability of the soluble crystalline salt ammonium sulphate [19]. Given that these requirements do not hold in every circumstance, the only way to truly determine whether or not a particle has an ice nucleating ability is experimentally.

There is still a lack of knowledge surrounding how biological aerosols aid ice formation, as there is considerable variation in ice nucleating ability. Hoose *et al* estimate that 1% of all bacteria and fungal spores (as well as 100% of pollen) belong to ice nucleation active species [20]. As well as this, it was approximated by Jaenicke *et al* that around 10×10^9 kg of primary biological aerosol particles (PBAPs) are emitted a year [21]. With such a considerable amount of material, it is important to establish the impact that PBAPs have on ice nucleation and hence cloud formation. As well as the aforementioned PBAPs, proteins can also make effective ice nucleators [22]. This is demonstrated in many arthropods and smaller organisms (insect eggs, mites etc). When overwintering, these organisms can be faced with subzero temperatures and if intracellular ice formation is allowed to occur it will most likely be lethal [22]. To avoid this, these creatures contain ice nucleating proteins which encourage supercooling causing extracellular ice formation at temperatures slightly higher than the hemolymph freezing point (the temperature at which the blood equivalent within an insect freezes). By doing this, it changes the osmotic balance and reduces the volume of water in the cells, reducing the freezing point of the intracellular fluid and delaying intracellular ice formation [23]. Alternatively organisms can also contain antifreeze proteins. Also known as thermal hysteresis proteins, antifreeze proteins lower the freezing point of water making them especially useful for saltwater fish as it lowers their internal freezing point below that of seawater [23]. In this thesis, one of the project investigated is whether Homogentisate 1,2-dioxygenase, commonly found in the liver, acts as an INP or an antifreeze protein.

The freezing point of seawater itself can also vary considerably and this will be the focus of the second project. As well as containing PBAPs, seawater has very high salinity which is maintained

even as it freezes into sea ice. The effect that salinity has on the freezing point depression of water is well documented [24] however the effect experienced when interacting alongside biological aerosols is uncertain. Furthermore, due to global warming and industrialisation there is an increased number of atmospheric pollutants having a potential effect too. With the impact of climate change being an immediate concern, it is important to establish the extent to which multiple potential INPs will have on the freezing point of seawater. In 2007, Serreze *et al*[25] reported that there was a decrease of around 100,000km^2 of sea ice per year and with rising temperatures that will only increase. If the salinity in seawater is contributing to this loss, it is vital to determine the impact.

For the majority of INP field sample collections, the samples are not analysed until they get back to a laboratory due to the instrumentation required. It would be more convenient however, to be able to test samples' ice nucleating ability before returning home so as to build up an accurate picture of their characteristics earlier and take multiple samples if necessary. To do this, a mobile cold stage would be ideal. Although not the most efficient, it would allow a basic determination of the freezing point of a sample without needing liquid nitrogen dewars or water cooling. It would become a valuable piece of field equipment. A mobile cold stage design is suggested in this thesis and experiments into its capability were conducted.

In this thesis, three separate projects were investigated. The first one involves the development of a mobile cold stage which can be further incorporated with microfluidics. The second is the analysis of Arctic snow samples to determine the effect of multiple INPs on the freezing point of sea water with a focus on the impact of salinity. The third is an investigation into the properties of the Homogentisate 1,2-dioxygenase enzyme to establish whether it has any effect on ice formation and if so, whether it falls into the class of an ice nucleating protein or an antifreeze protein. Preceding their presentation, this thesis contains an explanation of classical nucleation theory and how the equipment used works. The thesis is concluded with a summary.

CHAPTER 2

THEORY

2.1 Classical Nucleation Theory

Classical nucleation theory is a way of estimating the nucleation rate using thermodynamic quantities such as pressure difference and surface tension [26]. It can be used to model the nucleation of ice from supercooled water or supersaturated vapour as well as the formation of liquids from vapour [27]. All of the following equations can apply to any of these phase transitions, however in this thesis the focus will be on liquid water to ice formation. The majority of the explanation is derived from Murray *et al* [27].

2.1.1 Homogeneous nucleation

Homogeneous nucleation relies on cluster formation within the old thermodynamic phase. Above 0°C, this process is impossible but in supercooled water, it becomes more likely that a stable nucleus will be created as the critical size required to do so is reduced. On this stable nucleus, other particles will be deposited creating a crystal. To do this, the sample needs to reduce the phase transition barrier until it is of the same magnitude as the thermal energy [7]. The Gibbs free energy associated with forming a cluster is:

$$\Delta G_{cl} = \Delta G_s + \Delta G_v \tag{2.1}$$

where ΔG_s represents the free energy associated with making an interface and ΔG_v is the bulk term. Equation 2.1 can be rewritten as,

$$\Delta G_{cl} = -\frac{4\pi {r_i}^3}{3v} kT \ln S + 4\pi {r_i}^2 \gamma \tag{2.2}$$

where r is the radius of a cluster that contains i molecules, v is the molecular volume experienced when the species is in the condensed phase, k is the Boltzmann constant, T is temperature and γ is the interfacial energy between the old phase and the new phase. S represents the critical supersaturation ratio

and this can be found by looking at the ratio of liquid water vapour pressure over ice vapour pressure [28]. To calculate the critical radius for the cluster, the value of r_i needs to be found for which the derivative of ΔG_{cl} with respect to r_i is equal to 0. This gives,

$$r_g = \frac{2\gamma v}{kT \ln S} \tag{2.3}$$

Substituting this into equation 2.2 for r_i gives an equation for the Gibbs free energy of formation for a cluster of critical size:

$$\Delta G^* = \frac{16\pi\gamma^3 v^2}{3(kT \ln S)^2}. \tag{2.4}$$

Below the critical size for a cluster, the free energy will keep increasing relative to the cluster radius due to the dependence on interfacial energy. At small sizes therefore, clusters formed are unstable and will tend to dissolve.

To find a value for the rate of ice formation from a supercooled liquid, the Gibbs free energy of formation can be used in conjunction with the Arrhenius equation to obtain J, the rate of nucleation events per unit volume per unit time. The equation reads as follows:

$$J = A \exp \frac{-\Delta G^*}{kT} \tag{2.5}$$

where A is the Arrhenius constant representing the frequency factor. This A factor can be written in terms, $N_0 A_n q_0 Z$ where N_0 is a constant representing the total number of molecules in the system, A_n is the surface area of a cluster formed of n molecules, q_0 is the probability that a molecule in the liquid phase will have sufficient energy to become part of a neighbouring cluster and Z is the Zeldovitch factor. In this scenario,

$$Z = \sqrt{\frac{\Delta G_c}{9\pi kT n_c^2}} \tag{2.6}$$

and

$$q_0 = \frac{kT}{h} \exp \frac{-\Delta g^*}{kT} \tag{2.7}$$

where n_c refers to the critical size of the nucleus and Δg^* is the average height of the activation barrier met by a molecule when configuring itself in an ice-like structure. There are other ways of simplifying these equations that requires the assumption that the variables are not very temperature dependent. This allows the user to disregard A entirely and plot ln J against $T^{-3} \ln(S^{-2})$ instead [27]. This allows the interfacial energy to be calculated from the gradient without needing to know a value for A.

There are weaknesses within Classical Nucleation Theory, namely the assumptions that are required. Equation 2.2 assumes that a cluster is spherical, but given that ice crystals often form in hexagonal lattices or in lattices referred to as stacking-disordered (which means that the ice forms in randomised cubic and hexagonal layers [29]) the likelihood of a cluster forming perfectly is minimal. It also assumes that variables such as interfacial energy or saturation ratios have the same value on the nanoscale as they would macroscopically. With these variables, it is very possible that they are dependent on size [30]. Depsite this, CNT performs well in practice as demonstrated by its ability to accurately model bubble nucleation in polymer nanocomposite foams [31].

2.1.2 Heterogeneous nucleation

The results in this thesis require heterogeneous analysis due to the use of INPs. Heterogeneous nucleation occurs due to the presence of INPs which lower the free energy barrier. The equation for this process can be adapted from that for the homogeneous rate of nucleation. By including a new factor which represents the reduction in the free energy barrier, ρ, the equation becomes:

$$J = A \exp \frac{-\Delta G^* \rho}{kT} \tag{2.8}$$

where ρ can be defined as,

$$\rho = \frac{(2+m)(1-m)^2}{4} \tag{2.9}$$

where m is equal to cosϕ, the contact angle of the ice nucleus with a flat surface. This value is calculated by balancing the interfacial energies experienced by the nucleus. These energies are shown in figure 2.2.

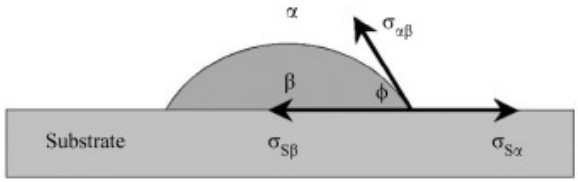

Figure 2.1: Diagram of the interfacial energies involved in calculating the contact angle

By using the energies shown, cosϕ can be calculated using:

$$cos\phi = \frac{\sigma_{S\alpha} - \sigma_{S\beta}}{\sigma_{\alpha\beta}} \tag{2.10}$$

where the σ values are the interfacial energies on figure 2.2. The nucleation barrier approaches zero when cosϕ approaches 1. For any angle $\neq$180° the nucleation barrier will be decreased. At 180°, the nucleus surface will not nucleate ice as it is energetically unfavourable. Equation 2.8 also differs from the homogeneous equation in its definition of the pre-exponential factor A. Rather than $N_0 A_n q_0 Z$ which was used for the homogeneous case, N_0 is replaced by N_s, the number of heterogeneous active sites present, or the number of molecules in contact with the surface. Even though the nucleation barrier is lowered by this interaction, there are fewer heterogeneous active sites present than homogeneous. The distribution of droplet sites can be modelled using single or multiple component stochastic methods. For single component stochastic (SCS) modelling, the probability of ice cluster formation is based on a single variable and is demonstrated as a randomly occurring event. Alternatively, a multi component stochastic (MCS) model can be used instead that represents a more detailed result for the distribution of active sites by taking multiple variables into account [27]. By including various factors simultaneously such as temperature, contaminants present and chemical composition of the particles, an increasingly accurate model of ice formation can be created. This is important to consider as the isothermal experiments will be affected by the number of sites present, and these models illustrate that the number is not always equal to the sample average.

It is hard to determine the exact quantity and catalytic ability of sites and hence the efficiency of heterogeneous active sites can be difficult to predict [12]. It has also been shown that effective active sites differ between types of heterogeneous nucleation mode. Hence, even if an INP is effective in deposition mode, it may not be as useful a catalyst in immersion freezing even at the same place on the nucleus [13]. This highlights the potential difficulties faced when modelling active sites. These active sites also present a potential weakness as equation 2.10 implies a flat nucleus surface. This is unlikely to be true due to INP's natural structures which feature many irregularities in texture, such as grain boundaries and pits all of which act as potential active sites. The geometries used to calculate the nucleation rate are therefore idealized.

The nucleation rate is also affected by the thermodynamics associated with ice nucleation including factors such as the release of latent heat and the final temperature achieved. These in turn are dependent on the degree of supercooling. The degree of supercooling, which is the difference between the temperature at which nucleation occurs and the equilibrium melting point [32], affects the release of latent heat during nucleation. The release of latent heat during nucleation is related to the energy required to form new interfaces between the liquid phase and the vapor or solid phase. The energy required to form these interfaces is known as the interfacial energy, and it is typically higher than the energy required to form the bulk of the new phase. Therefore, the release of latent heat is due to the conversion of the higher energy interfacial area to lower energy bulk area, resulting in an overall decrease in the system's energy. A higher degree of supercooling results in a larger release of latent heat because more energy is required to form the new interfaces. This means that the energy released during nucleation is proportional to the degree of supercooling. The final temperature achieved after ice nucleation also depends on the amount of latent heat that is released and the cooling rate of the sample. The more latent heat that is released, the higher the final temperature will be. On the other hand, a faster cooling rate will result in a lower final temperature. Understanding these factors is important in being able to model the rate of ice nucleation.

2.2 Dynamic Light Scattering

Dynamic Light Scattering measures the diffusion behaviour of the molecules in a solution to determine their sizes. As the diffusion behaviour depends on the size of the macromolecules, determining the diffusion coefficient allows the radii of molecules to be found. This next section largely follows an explanation by Stetefeld *et al* [33] and will be used to describe the theory and data analysis associated with dynamic light scattering.

To find the size of a macromolecule using DLS, a laser light is shone at the sample. The light will scatter when it encounters a molecule and the intensity of the scattered light is recorded by a detector. The diffusion rate can then be found by how frequently the intensity fluctuates. Larger particles will diffuse more slowly and therefore the intensity will stay relatively stable at a position where there is a large particle. Where there are smaller particles, the intensity will fluctuate rapidly due to the higher speed of diffusion. Knowing the viscosity, the diffusion coefficient can be used to find the size of

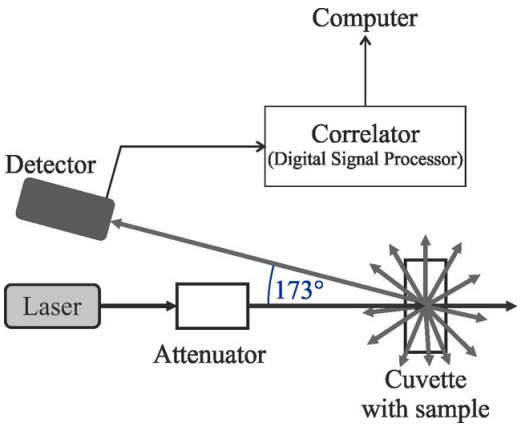

Figure 2.2: Diagram of the components of a DLS taken from Eberhard [2]

macromolecules.

A key quantity is the Electric Field Correlation Function and is defined as:

$$G_1\langle\tau\rangle = \langle E(t)E(t+\tau)\rangle \tag{2.11}$$

where τ is the delayed time and both variables are equal to the scattered electric field at times t and (t + τ) respectively. A second correlation function is also required to relate the intensity to the movement of the molecules in solution. This is a very similar form to equation 2.11 and reads as follows:

$$G_2\langle\tau\rangle = \langle I(t)I(t+\tau)\rangle \tag{2.12}$$

where I is the intensity at those two points. Combining these two correlation functions helps to define a diffusion constant. By using the Seigert relation, the equations can be rewritten as:

$$g_2(\tau) = B + \beta \mid g_1(\tau) \mid^2 \tag{2.13}$$

where B is a baseline value, normally approximate to 1 and β is a variable representing detector area, optical alignment and scattering properties usually referred to as the coherence factor. The electric field correlation factor experiences decay over time and polydisperse systems exhibit a distribution of decay rates due to the various sized particles in solution. As the system investigated in this thesis is polydisperse, the monodisperse solution will not be considered. The integral representing this distribution (G(Γ) can be seen below:

$$g_1(\tau) = \int_0^\infty G(\Gamma)e^{-\Gamma_\tau}d\Gamma \tag{2.14}$$

where Γ is the decay constant. This value is related to the diffusion coefficient (D) by:

$$\Gamma = -D_\tau q^2 \tag{2.15}$$

where q is the Bragg wave vector and equal to:

$$q = \frac{4\pi n}{\lambda} sin\left(\frac{\theta}{2}\right) \tag{2.16}$$

where n is the refractive index of the dispersant, λ is the wavelength of the incident light (laser) and θ is the scattering angle. Using this relation, the diameter of the particle in solution, *d(H)*, can be found using the Stokes-Einstein equation:

$$d(H) = \frac{kT}{3\pi\eta D} \tag{2.17}$$

where k is the Boltzmann constant, T is the absolute temperature, η is the viscosity and D is the diffusion coefficient. As this diameter refers to the hydrodynamic diameter of the particle, the value depends on several other variables such as the ionic strength of the medium and the surface structure and shape of the species. If the medium has a very low conductivity, it will give the appearance that the particle is larger due to an increase in the Debye length, the thickness of the electric double layer. When the conductivity is low, the electric double layer expands, reducing the diffusion speed and causing the DLS to report the particle as larger than it really is [34]. This is part of the reason why it is important to calibrate the DLS instrument with latex spheres of known size before results are collected.

The shape of a particle can affect the diffusion constant, hence the DLS returns a hydrodynamic diameter that is the same size as a sphere with the same diffusion coefficient [34]. This makes the results slightly inaccurate if dealing with anything such as a polymer or a protein so the results in this thesis are used as a relative measure rather than an absolute one.

Once the physical experiment has taken place the results are calculated using analytical distribution methods. There are two scattering theories that are used in this calculation, Rayleigh scattering and Mie theory. Rayleigh scattering applies when the particles are smaller than the wavelength of light (approximately 10 times smaller). When this is the case, the laser light will be scattered isotropically. The intensity that will be collected from this scattering will be proportional to (radius)^6 meaning that often the intensities from small particles are vastly overshadowed by the intensities from larger particles that are present. Mie theory is relevant when the particles are around the same size as the wavelength of the laser beam. This is the theory used in most DLS instruments as it provides the most accurate results.

The constrained regularization method for inverting data (CONTIN) is one of the most popular data analysis methods that requires an adapted version of the non-negative least squares (NNLS) method. CONTIN provides an intensity size distribution which is a demonstration of the various particle size and the corresponding intensity of scattered light from each one. The intensity-weighted distribution can be seen below:

$$\%I_a = \frac{a^6 N_a \cdot 100}{N_a a^6 + N_b b^6} \tag{2.18}$$

where N_a represents the number of particles of size a. Using Mie Theory, the intensity-weighted distribution can be converted into a volume-weighted distribution. By recalling Rayleigh scattering, where intensity is proportional to (size)^3 and assuming that the density is uniform, the following equation is created:

$$\%V_a = \frac{a^3 N_a \cdot 100}{N_a a^3 + N_b b^3}. \tag{2.19}$$

This equation provides the distribution that will be used in the DLS results for this thesis as it represents the volume proportion of multiple species in a sample. For this project, this was the most useful factor

as it could identify aggregation. For this equation to work however, assumptions had to be made. It assumes that all particles are spherical and homogeneous, that they have a uniform density, as previously mentioned, and that the refractive index is known [33]. This is potentially where uncertainties will occur, as the samples in this thesis are proteins and are likely not perfectly circular. However, the results used were relative, therefore they still provide useful information.

CHAPTER 3

AUTOMATED LAG-TIME APPARATUS

3.1 Introduction

The Automated Lag-Time Apparatus (ALTA) used in this thesis was developed by Fred Cook at the University of Bristol based on a design by Barlow and Haymet. When it was first created by Baldwin and Vonnegut, it's original purpose was to freeze-thaw samples many times to observe the time that elapsed before nucleation occurs [3]. This helped establish that there is a stochastic freezing pattern of nucleation. By freezing and thawing multiple times, statistical variations can be eliminated as it allows more data points to be collected. In further papers, Baldwin and Vonnegut also highlight that freeze-thawing can alter the nucleating agent, often resulting in different nucleation times. Their experimental set up can be seen in figure 3.1. This equipment is relatively simple compared to future versions but was automated and functioned well.

The sample was placed in the bottom of the U-tube and immersed in a solution of water and ethylene glycol, cooled to below 0°C. When the sample began to freeze in the lower section of the tube, the electrodes detected a large increase in electrical resistance since the freezing prevented the movement of ions. This then triggered a solenoid to remove the tube from the bath and begin warming the sample with a hair dryer. When the water had melted, the U-tube was returned to the cold bath so the cycle could start again [3]. This method was improved upon by Barlow and Haymet.

Barlow and Haymet's experimental set up replaced the U-tube with two individual chambers, one containing the sample and one containing an antifreeze sample (specifics not given in the research) and a thermocouple. This is so that the temperature can be measured in the second chamber without disturbing the freezing in the first. These are then placed into a bath with a water supply that can vary between cold and hot water so that the freeze-thaw process can be run. The main difference between Barlow and Haymet's and Baldwin and Vonnegut's equipment is the determination of nucleation. Rather than measuring a resistance increase using electrodes, the new method uses a laser and a phototransistor.

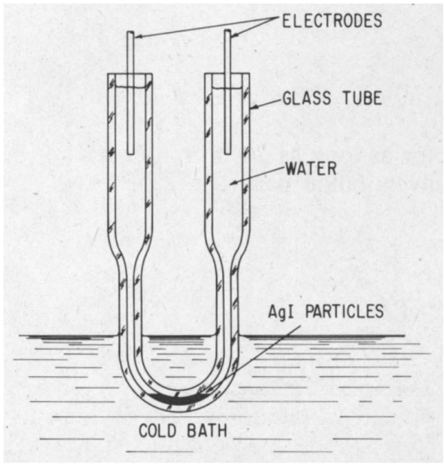

Figure 3.1: Diagram of the experimental set up used by Baldwin and Vonnegut in their version of the ALTA [3]

When the sample freezes, the amount of light reflected increases. Based on the voltage received by the detector, the solenoid valves can either continue to cool the sample using the cold supply or warm the sample using the hot. Hence, the freeze-thaw process can continue automatically [35].

To create the ALTA equipment that was used in this thesis, Fred Cook[4] adapted the nucleation determination method from Barlow and Haymet creating a device that was self contained. Instead of a laser and a phototransistor, an LED and an LDR were used. The two components are placed on either side of the sample. When the sample freezes, the opacity increases and the amount of light reaching the LDR decreases and changes the resistance experienced. When this occurs, the device can begin re-heating the frozen sample. As well as this, the method of placing the sample in a water bath was also adapted, opting instead to heat and cool the system using Peltier coolers. A Peltier cooler creates a temperature difference by flowing current through alternating p and n semiconductors, removing heat from one junction and depositing it at the other [36]. This creates a cooling effect on one side of the cooler and a heating effect at the other. Although they are not very efficient, they are convenient, compact and allow precise control of the temperature which water baths do not. The temperature of the system is recorded using a Platinum Resistance Thermometer (PRT) that is permanently located in a separate compartment just below the sample. To calibrate the equipment, a second thermometer would be placed into the sample holder to determine the temperature experienced in that position and identify if there is a difference between the two values being read by the thermometers. This method benefits the experiment as the permanent thermometer is non-invasive meaning that it will not interfere with the nucleation. It also provides a calibration method that is accurate and reliable for the day of the experiment as unlike a water bath, the conditions of a Peltier cooler are unlikely to change within the day. The temperature may affect the efficiency of the cooler (the hotter it is, the harder it is to remove heat from the junction) however within the time taken for the experiment to run, this is minimal.

In this chapter, the ALTA is adapted again to provide a system that can be used for isothermal or

frozen fraction experiments with multiple droplets at a time. The previous configurations of the apparatus have used a large sample volume which is useful when a small sample volume would take too long to freeze however it also increases the likelihood of being dominated by contaminants and takes longer to obtain statistically significant results. The new version of the ALTA can measure linear or isothermal freezing for up to 20 droplets at a time from a compact and easily transportable device. Furthermore, it will be able to incorporate microfluidics in the future which will allow observation of droplet freezing on a much smaller scale. This would be very useful as it enables nucleation rates to be measured without assumptions or the risk of serious contamination, and it provides the ability to study single crystals (such as $CaCO_3$) due to its capacity to control diffusion, concentration, flow dynamics and the interfaces experienced by the droplets [37]. This is a promising idea and would be very valuable to researchers both in universities and out on expeditions where space is limited.

3.2 Experimental Method

The ALTA was built and programmed by Fred Cook as part of his PhD thesis. Many trial runs of the original version were conducted to determine the minimum temperature the sample could reach and allow a greater understanding of how the existing interface and hardware functioned. In figure 3.2 the original structure can be seen with an aluminium sample holder positioned between two peltier coolers on either side with a fan to extract the heat produced. The hole in the top holds the sample and the two on the front face hold the LDR and the PRT respectively. A schematic of this design can also be seen in figure 3.3. It was established that the best way to run experiments that determined minimum temperature was to program isothermal tests rather than linear temperature ramps. These allow the ALTA to cool for as long as possible as fast as possible.

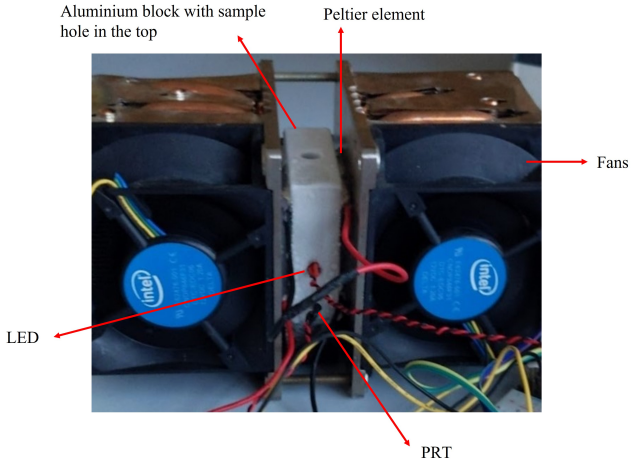

Figure 3.2: The original configuration of the ALTA built by Fred Cook

To obtain the results required for this project, the hardware had to be opened up so that the peltier coolers were lying flat on the top of the fans, parallel to the table. This can be seen in figure 3.4 and

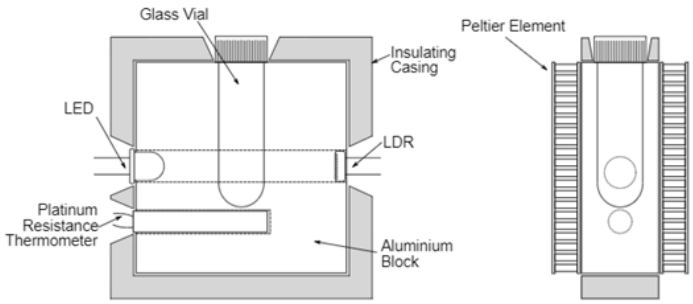

Figure 3.3: A schematic of the original configuration of the ALTA built by Fred Cook. Fans are placed on either side of this set up to remove heat from the Peltier coolers [4]

provided a flat surface for samples to rest on whilst in full contact with the cooling mechanism. At this point, more test runs were conducted to observe the minimum temperature that the system could reach when only one peltier cooler was in contact. It was tested with both the PRT placed inside the aluminium block on top of the peltier cooler and with the PRT held directly on top of the peltier. The results indicated that the aluminium prevented the most effective cooling of the sample and hence had to be removed. To continue the investigation into the minimum temperature that could be reached by the

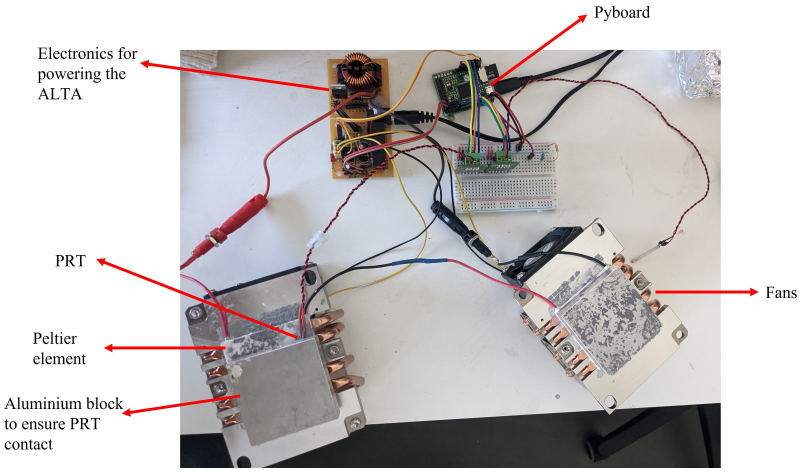

Figure 3.4: The ALTA deconstructed so that the peltier coolers are flat and can have a sample placed on them

system, the python script had to be altered so that it did not depend on the LDR. As the experiment is not enclosed in the new set up, the experiments were stopping too early due to readings by the LDR that would indicate the sample was frozen. This was because the LDR was only ever reading ambient light and not actually in use. Removing this factor from the script meant that isothermal experiments could be run for as long as was required without interference. Next, experiments were set up using two different thermally conductive pastes to optimise the set up to achieve the coldest possible temperature in the

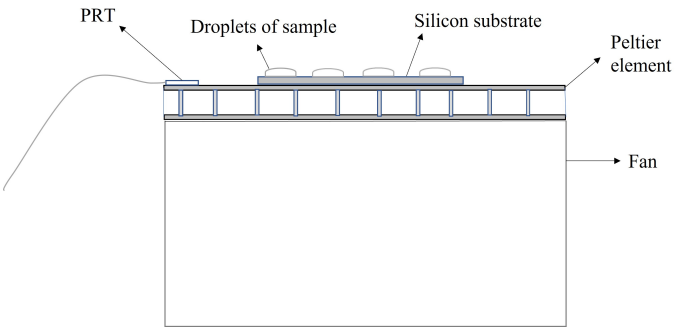

Figure 3.5: A schematic of the new ALTA configuration so a sample can be observed

fastest time. To do this, the python script was instructed to run an isothermal experiment at -40°C for 10 minutes. The -40°C was an arbitrary target to ensure the actual minimum temperature of the system would be achieved. The PRT was placed on top of a layer of thermally conductive paste on the peltier cooler. It was held down by placing the aluminium block on top of it just to ensure complete contact. These experiments were run with both silver epoxy and a product called MX4, a silicone compound containing carbon nanoparticles which is used for thermal conduction in PCs. The thermal conductivities associated with these products are 1.55W/mK and 8.5W/mK respectively. The experiment was run with just the thermal paste the first time and was then run again using foil wrapped polystyrene as insulation. The block of polystyrene was shaped to fit around the aluminium holding the PRT and was then placed on top, ensuring that it did not cover any part of the Peltier cooler. If the polystyrene was placed so it enclosed the peltier cooler too, the heat from the opposite side of the peltier would begin to warm the insulation, to the detriment of the experiment. This was done to observe whether insulating the aluminium would have an impact on the minimum temperature the equipment could achieve.

After the ideal configuration had been established, the ALTA was tested to see if it could freeze a sample of K-feldspar and be observed using the microscope camera. A pre-made solution of K-feldspar of unknown provenance was found in the laboratory and used for this test run. A substrate made from a silicon wafer was used and was placed on top of a layer of MX4 on top of the peltier cooler. On this, μL droplets were pipetted onto the substrate and it was placed under the microscope. The full method of creating a droplet array is discussed in detail in Chapter 5. The python script was programmed to run an isothermal experiment and hold the sample at -12°C for 10 minutes. The camera started taking pictures once the sample was at -12°C and the freezing of the droplets was recorded.

3.3 Result

The results from the use of different thermally conductive pastes can be seen below in figure 3.6. Where the name is followed by a '+', it indicates that the polystyrene block was used as insulation at the same time. This graph clearly shows the efficacy of MX4 compared to the silver epoxy as it could reach temperatures down to -20°C over twice as quickly. After 10 minutes, the MX4+ was at -28.7°C whereas

silver epoxy+ reached -22.4°C in 10 minutes. The MX4+ achieved this latter temperature in 64 seconds. The polystyrene insulation has a significant effect for the silver epoxy. It has less of an impact for the MX4 as the rate is already very fast. MX4 is definitely the better choice to use for experimental purposes. For isothermal measurements, the sample has to reach the holding temperature as quickly as possible to reduce the number of droplets that freeze prematurely as they will not count in the results. The rate of cooling for silver epoxy is therefore far too slow, even with the use of insulation.

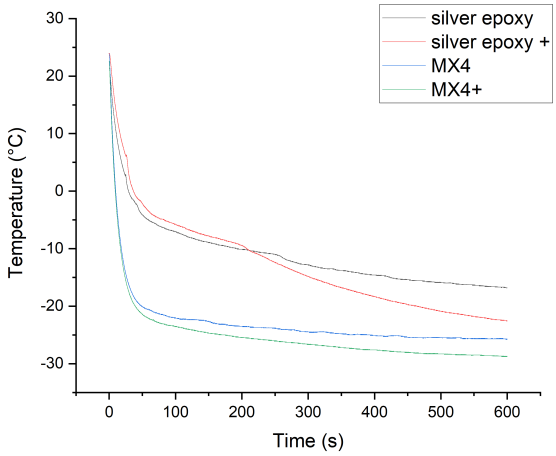

Figure 3.6: A graph showing the effects of different thermally conductive pastes on the cooling rate of the ALTA. The + indicates that polystyrene insulation was used at the same time

Unfortunately, due to software issues, the ALTA did not hold the temperature during the K-feldspar test as desired. This issue could be resolved through a rewriting of the Python code which would have been completed if not for time restraints. Figure 3.7 below is an image taken of the K-feldspar droplets during the experiment with three frozen on the left. This figure demonstrates that the ALTA is capable of conducting these experiments as the hardware is fully functioning. It is only the software that is required to be altered. In future experiments, a brighter light source would also be useful in better illuminating the droplets.

3.4 Conclusion

To conclude this section, the results collected from the ALTA demonstrate a strong step towards adapting the equipment for use with microfluidics and a larger sample set. The use of the MX4 thermal conducting paste allowed much lower temperatures to be reached than previously achieved. This version is useful to be able to gather statistically valuable data as well as providing the ability to study the ice nucleating effect of single crystals of species such as calcium carbonate. To further improve this equipment, the software needs to be edited to hold the temperature successfully, a better light source needs to be introduced and ideally, the PRT should be attached to the cold stage to ensure perfect contact.

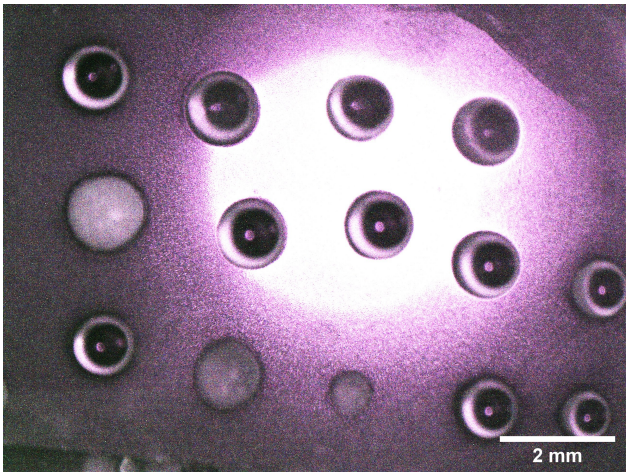

Figure 3.7: A sample of K-feldspar being frozen by the ALTA in an isothermal experiment

CHAPTER 4

BRITISH ANTARCTIC SURVEY

4.1 Introduction

In the last twenty years, the sea level has risen by more than 5cm worldwide [38] with Antarctica losing 152 billion tons of ice mass per year [39] through global warming. Among the more publicised effects of climate change, there are many other variations that are not as familiar, such as increased ocean salinity. With a higher salt content, the climate will begin to warm due to a reduction in sea ice coverage [40], lowering the albedo and resulting in warmer atmospheric temperatures [41]. Sea ice forms naturally in both the Arctic and the Antarctic when it is cold enough for the sea to freeze and is vital for maintaining a stable climate as it reflects sunlight back into the atmosphere and traps the existing heat in the ocean. As well as this it helps with ocean circulation, a process also impacted by increased salinity due to the effect it has on the density of the seawater [42]. The creation of sea ice begins with the formation of small ice crystals called frazils which float on the surface until the crystals critically expand and form a suspension. These ice crystals are compacted during periods of rough weather and form structures called pancake ice. Given this name due to their large circular shape, pancake ice can be further compressed into sea ice floes when they collide with other pancakes on the oceans surface. Sea ice floes can be up to five kilometres wide and carry fresh snowfall wherever the oceans currents take them. Snow on sea ice floes gain salinity through a process known as upwards migration even though the salt content of the sea ice itself is reduced compared to the seawater it is formed from. During freezing, the sea ice discards the salt through brine rejection. This rejection occurs as the floes travel on the open water. They continue to grow as the water below them freezes to the underside through congelation growth [43]. Simultaneously, the atmosphere cools the upper side, freezing pockets of seawater and air created during the growth and condensing them into brine. As the floe grows larger, the brine is ejected from the ice and increases the salinity of the seawater below it [43]. The snow on these floes are the subject of this investigation alongside a sample collected from the lead, the area of open water between floes.

With salt content clearly having an impact on the climate of the Earth's oceans, this project aimed to analyse the effect it had on the freezing point of freshly fallen snow samples taken from the Arctic and then melted in the laboratory. Primarily, the snow would experience salinity due to upwards migration from the sea ice however it is also possible that it occurs from deposition. By investigating the extent to which the salinity from upwards migration affects the freezing point of snow, compared to other factors such as pollution or even salinity transported via sea spray, the impact that these methods have on the immersion nucleation of snow can be assessed. If the freezing point is depressed significantly by the salinity it will have an impact on the formation of sea ice as it will require a lower temperature to freeze. This will reduce the rate of formation and potentially lower sea ice coverage even further which would be hugely damaging for the planet.

The MOSAiC (Multidisciplinary drifting Observatory for the Study of Arctic Climate) expedition took place from September 2019 to October 2020 and was designed to investigate the Arctic's climate system. During this time, snow samples were collected from snow pits and refrozen port lead by the team at the British Antarctic Survey (BAS) and were brought back from the research vessel Polarstern to Cambridge to be analysed. As these samples were taken at different heights from the highly saline sea ice, the greatest factor of interest was the effect of salt content on the freezing point. The samples were tested for ion concentrations and were then required to be tested for their freezing temperatures to establish the extent of the INPs individual impact on the freezing point recorded. Alongside these results, multiple tests into the ideal working conditions for the equipment used at BAS were conducted. The Linkam Cold Stage required calibration and scientific evidence that the results were repeatable and hence experiments were also carried out to determine these aspects.

In this chapter, the most suitable conditions for attaining results with the Linkam cold stage are discussed as well as supplying a calibration value so future measurements can be corrected accordingly. Additionally, results displaying the correlation between multiple INP concentrations, the samples height above the saline sea ice and their freezing points are displayed for six separate MOSAiC samples, each collected from different depths. Through thorough analysis, ideas are presented for why the results follow particular trends and why they may not be quite as expected.

4.2 Experimental Method

4.2.1 The Equipment

For all of the experiments conducted at the British Antarctic Survey, the Linkam LTS120 Cold Stage was used. It uses a Peltier system on a temperature controlled cooling stage made of pure silver [44]. The sample can be placed directly on to the cooling stage ensuring a good thermal connection. The temperature for this particular cold stage is controlled with the help of a water circulation pump. It had to be turned on 20 minutes prior to experimentation to allow the water to be cooled from room temperature (~20°C) to 5°C. At this ambient temperature, the water is circulated and provides a temperature gradient that the Peltier system requires for both heating and cooling.

The experimental set up can be seen in figure 4.1. The Linkam Cold Stage is attached to a white board that has a hole in each corner. These holes are colour coordinated with the legs of the camera set up to ensure that the images taken are always the same orientation.

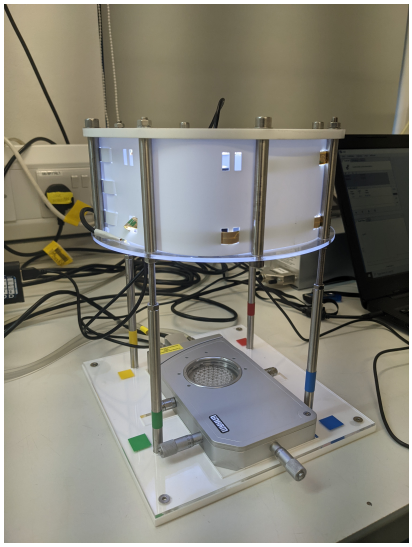

Figure 4.1: The BAS cold stage set up featuring the Linkam Cold Stage underneath a camera/LED lighting system

An example of the droplet array created in each experiment can be seen in figure 4.2. The code assigns each droplet placement a number and although possible to reassign these, it is much more convenient to try and ensure that all of the images have an orientation as close to that of figure 4.2 as possible. When the droplets are clearly visible in their designated spot, the code is able to identify their freezing points accurately using the opacity change. With multiple data sets, where there are 60 droplets each, this is a valuable time saving measure. It is therefore important that the placement of the sample is always the same.

Further details of the experimental set up can be seen in figure 4.3. Below the swinging lid of the Linkam cold stage sits the silver cooling stage which can be seen as the square in the centre. To stabilise the sample, a plastic holder cut to the shape of the stage was used that had two metal pins which sat in the base of the stage. This ensured the sample did not move during the sensitive process of pipetting the droplets. Directly on top of the cooling stage, in the circle of the holder, a glass slide was placed using vacuum tweezers and immediately on top of that was the specially made plastic droplet separator. This slotted in to the holder and provided 60 individual slots for the droplets that prevented contamination and ensured that the droplets would not spread or join with other droplets. Droplets of 1μl were carefully pipetted into each of the 60 spaces in the separator. When this was finished another glass slide was placed on top of the separator and the swinging lid was closed. The whole cold stage was placed correctly underneath the camera and the stage was lit by LEDs within the camera system. Surrounding this, a makeshift cover was created to shelter the set up and make sure all the reflected light was kept within the cameras field of view. The droplets need to be very well lit for the code to detect their opacity so

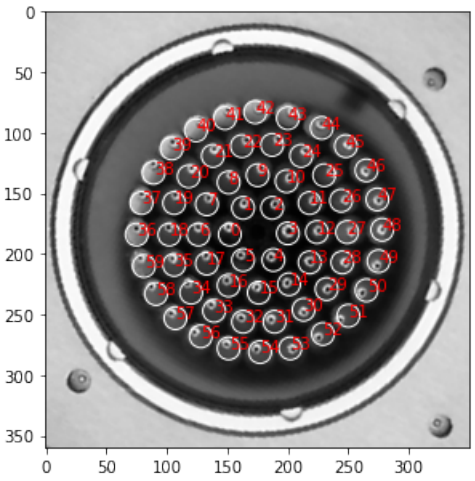

Figure 4.2: An example of a droplet array image and the numbered places designated by the code for each of the 60 droplets

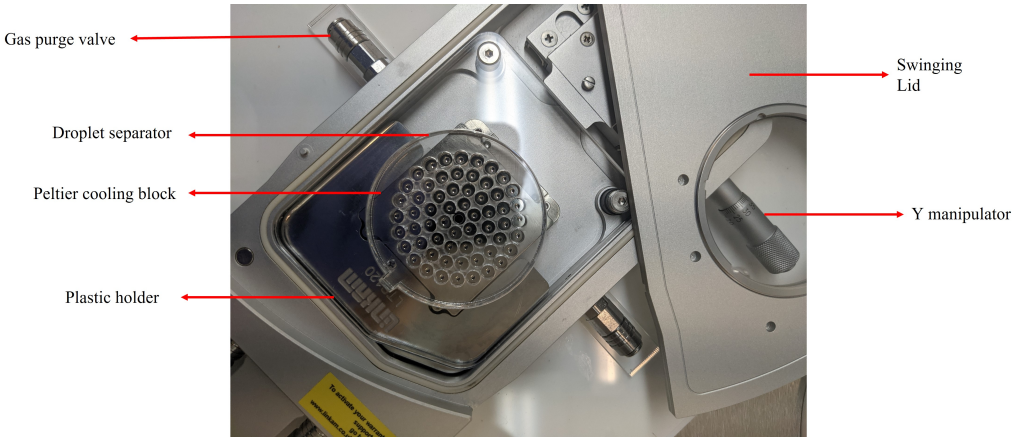

Figure 4.3: A close up of the Linkam cold stage set up showing all of the individual components and how the array was placed on the cold stage

isolating the system ensured the images were the best quality possible. The cover can be seen in figure 4.5. It was simply made from a folded piece of paper and a piece of fabric by the team at BAS.

After the experiment was complete, every component had to undergo thorough cleaning.The plastic parts (holder and separator) were removed from the system and were rinsed with MilliQ water. After this they were placed in a container filled with MilliQ water and were sonicated in an ultrasound water bath for 30 minutes at 21°C. When this was finished the containers were drained and they were placed on lint free paper towels under the fume hood to finish drying. All glass slides used in the experiments were disposed of after use. The cooling stage itself was wiped with acetone and isopropanol using a lint free cloth before each new experiment. If there was any risk of contamination of either the mechanical tweezers or the tip of the vacuum tweezers during the set up they were also cleaned using the sonication

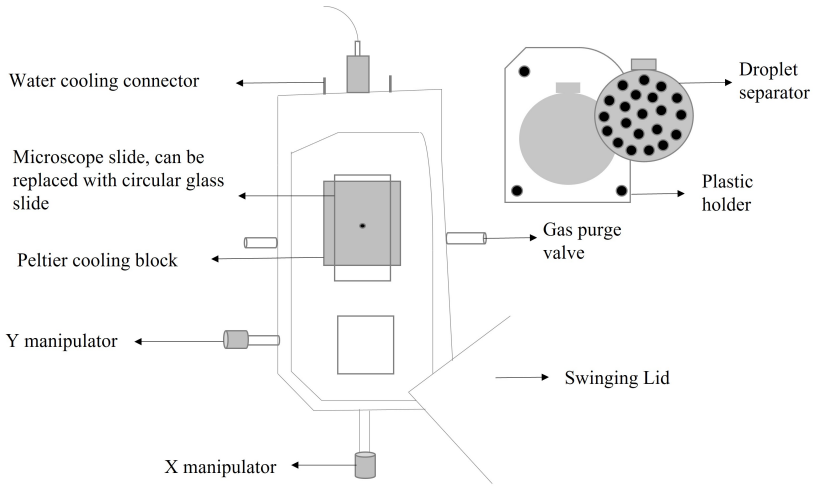

Figure 4.4: A schematic of the Linkam cold stage, including the droplet separator and plastic holder used for these specific experiments

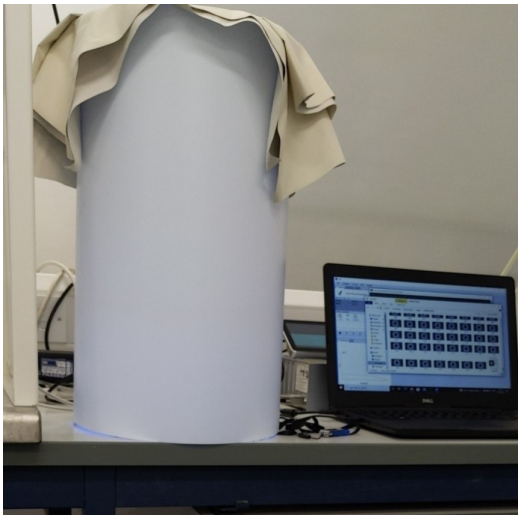

Figure 4.5: The light isolation cover used for the experiments

method. The surface of the fumehood was also wiped with isopropanol in between experiments.

4.2.2 Calibration

As it is unknown where the temperature reading is taken within the cold stage, it is possible that the temperature being recorded and the temperature being experienced by the samples are different. To ensure that the Linkam cold stage was reading the correct temperatures, a calibration test was run twice. To calibrate the Linkam cold stage, a sample of MilliQ water with a known melting point of 0°C underwent a three stage temperature ramp with the equipment set up as previously described. It was cooled very quickly (20°/min) to -30°C, freezing the sample, heated at 10°/min until -5°C followed by a

last temperature ramp of 1°/min until 8°C. Using a slow ramp in the final stage allows the camera to pin point an exact melting temperature for every droplet.

The experiment itself was run using an Anaconda Powershell prompt window. From this, the camera could be controlled. Images were taken every 2 seconds and these were used in the analysis to determine melting point. Images were recorded from the start of the 1°C /min ramp to ensure that enough data was collected without taking up too much computational storage.

4.2.2.1 Frozen Fraction

Frozen fraction refers to an investigation into the temperature at which 50% of the droplets have frozen giving a median value. The first frozen fraction experiments were run using MilliQ water to prove the repeatability of the results and the precision of the equipment. In total, MilliQ water was run 5 times with a new sample each time. These runs were also used to enable the ideal experimenntal conditions to be found. For example, in the first run, the camera was taking pictures every 0.2 seconds resulting in a total of 10,000 images from a single run. This is unsustainable in terms of computational expense and ease of analysis. A balance needed to be found to guarantee that pictures were recorded frequently enough to document an accurate freezing time (and hence temperature) for the droplets whilst also not making the data files unreasonably large. In the end, the decision was made to record images every 2 seconds. Similarly, a compromise needed to be found for the rate of the temperature ramp. The MilliQ water, (apart from the very first run at 5°C/min) were all run at 1°C/min for the entire freezing process. For later experiments, as with the calibration, the use of multiple temperature ramps meant that a degree of accuracy could be achieved whilst also optimising time efficiency.

For the MOSAiC samples, only sample BAS-1476 was run with a temperature ramp of 1°C/min. Every other sample had runs taken using multiple temperature ramps, however this should not affect the results as at the relevant freezing temperatures, the ramp was the same. The temperature ramps used to measure the frozen fraction in these experiments was 1 at 3°C/min until -10°C, 1 at 1°C/min until -30°C. Before the samples were pipetted onto the glass plate, they were defrosted in the fumehood. When fully melted they were then shaken for 10 minutes using a laboratory shaker. This should ensure that any potential INPs were diffused within the sample. They were then decanted into smaller vials. If the vial had sat for a while before being used for a repeat trial it was shaken by hand before being used again. After this, the samples were frozen at the temperature ramps previously stated and the images recorded ready for analysis.

The measurements for the ion concentrations used later in this chapter were taken by Dr. Markus Frey and his team at the British Antarctic Survey. To acquire the results, ion chromatography was used. Due to the high salinity, the snow samples were diluted with ultra high purity (UHP) water by a factor of 100 before they were separately analysed for major ions, cations and anions [45].

4.3 Results

4.3.1 Calibration and repeatability

The results for the calibration are demonstrated below in Figure 4.6. This graph is for the second run that took place, however it demonstrates the consistency of the melting temperature of the droplets.

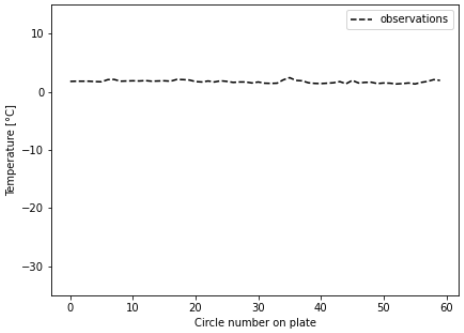

Figure 4.6: The melting temperature observed for every droplet on the cold stage for the second calibration run

The melting point of the MilliQ water (a pure water) was found to be 1.9°C and 1.7°C for each run portraying a systematic error causing the value to deviate from the true melting point of 0°C. Interestingly, both of these results indicate that the cold stage is recording the temperature almost 2°C too warm which could have a notable effect on values for future samples. For the purpose of these repeatability results, an average of 1.8°C was used to correct values.

The results can be seen in figure 4.7 and the median values (temperature when half the sample had frozen) are as follows: -30.0°C, -27.6°C, -27.3°C, -29.0°C and -27.7°C. The first result is considerably lower than the rest and this is due to the cooling ramp being set to 5°C/min which meant that the exact temperature of droplet freezing was less accurate than the following runs where a ramp of 1°C/min was used. When cooling ramps are faster and the image rate is the same, the exact time for freezing is rarely captured as by the time the image is taken, the temperature may have decreased by an extra 0.2 °C. As well as this, given the stochastic nature of freezing, generally the slower the cooling rate the higher the probability of freezing and this may have skewed the result. For this reason, the first result can be considered an anomaly. The fourth result of -29.0°C can also be considered an anomaly due to the formation of condensation under the glass screen. Although this doesn't affect the freezing temperature it does affect how accurate the analysis is as the droplets are much harder to see. This fourth run had the shortest time out of every sample for the cold stage to warm back up to room temperature (about 15 minutes as opposed to the 30-60 minutes that the other runs had). Due to this, the condensation present is greater and the result is less accurate. Removing both of the anomalies from this data set gives three very consistent freezing temperatures for MilliQ water. The average result comes to -27.6°C which, with the calibration correction, is a final value of -29.4°C indicative of a pure water.

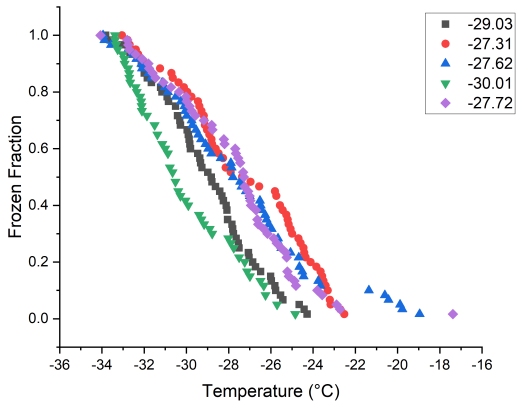

Figure 4.7: Frozen fraction results for five runs of MilliQ water to test the repeatability of the equipment

4.3.2 MOSAiC samples

MOSAiC Samples		
Sample number	Average freezing temp	Distance above sea ice
0036	-25.9°C	26.5cm
0656	-28.2°C	20cm
0839	-29.0°C	18cm
0774	-25.0°C	14cm
0666	-24.8°C	9cm
1476	-25.6°C	recently fallen on lead

Table 4.1: Table displaying the temperature taken when 50% of the sample had frozen as well as the distance above the sea ice each sample was collected from

The fundamental data for each of the six MOSAiC samples analysed can be seen in table 4.1. As the location is given in terms of distance above the sea ice, the sample with the largest distance (0036) represents the sample collected closest to the snow layer surface and the open air. The average freezing temperature for each sample was also calculated by determining the temperature when 50% of the droplets in the sample had frozen, providing a median value. Each sample was also run using fresh droplets at least three times to ensure that the data being collected was repeatable and accurate. An example of this can be seen in figure 4.8 where the experiment was run three times but provided clear evidence of an anomalous result. It also seems there are two populations of nucleating agents acting on that particular sample given its two-step appearance. This result was discarded and anywhere an outlier appeared, it was removed from the data set. Some of these occured due to the formation of condensation in the cold stage however a full discussion into the experiment will follow this section. A graphical

representation of all data samples can be seen in figure 4.9. When demonstrated visually, the difference in freezing points between samples 0839 and 0656 compared to the rest of the data sets is clear.

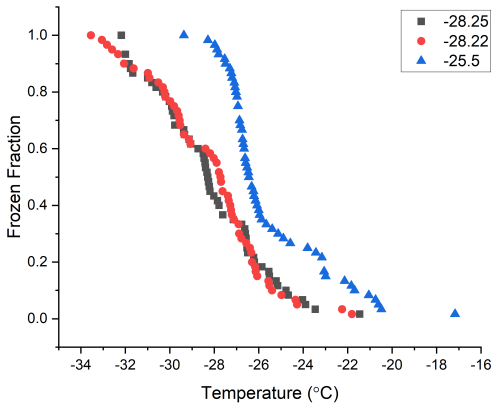

Figure 4.8: The results from three experimental runs for sample BAS0656 and the demonstration of an anomalous result

When looking at the distance above sea ice for these two samples, they are found in similar areas and are relatively close to the surface without being at risk from contaminants. With average temperatures around -28.5°C, and using the calibration data to correct this value to -30.80°C in the case of BAS0839, these samples have a freezing point similar to a completely pure water. They appear to be high enough above the sea ice to limit the effect of upwards migration and are far enough from the surface to not experience pollutants. The rest of the samples all provide a very similar freezing temperature regardless of their location, although the ion concentrations they are carrying are very different.

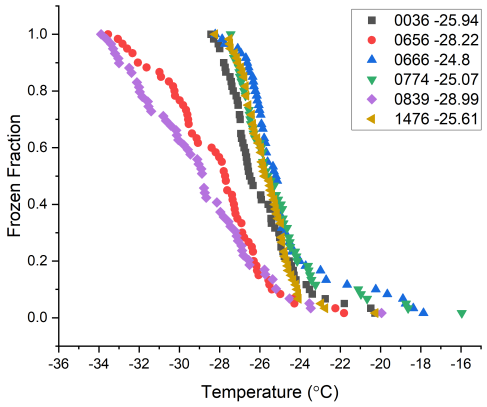

Figure 4.9: The frozen fraction data for all six MOSAiC samples along with their average freezing temperatures

Figure 4.10 demonstrates the correlation between freezing temperature and chloride content for each of the six samples. For the purposes of these results, sample 1476 is displayed as 30cm above sea ice as it was fresh snow collected from the surface and an actual distance was not provided for it. The correlation with salinity is not as expected. For the first sample closest to the high saline sea ice, it has a significantly higher salt content than the other samples however its freezing point does not seem to display any freezing point depression. A freezing point depression would be expected due to the colligative effects experienced when a solid solvent is added to a liquid solvent. In the case of these samples, as they are known to contain impurities, it is expected that as the concentration of the INPs increase, the freezing point will be lowered. However, the effect of freezing point depression is actually more minimal than expected. For sea water with a value of 19.35g/kg (equivalent to over 19 million in parts per billion weight) the freezing point depression is only expected to be around -1°C [43]. Therefore, although this sample has a high chloride content relative to the others at 69000ppbw, it is actually still very low comparably. Looking at this result suggests that the sample contains another INP that may increase the freezing point rather than depress it as salt does even if the effect is negligible. As

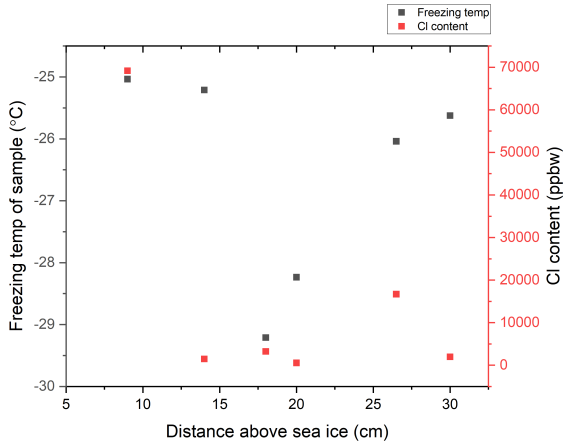

Figure 4.10: The chloride content of each sample displayed alongside their freezing temperature and distance above the sea ice

well as the sample at 5cm, the samples at 18cm and 20cm also do not seem to experience a freezing point depression from chloride. It is surprising that the sample at 18cm would have a freezing point as low as -28°C when the salt content is so low and similarly for the sample at 20cm. There are possibly other contaminants that are affecting these two samples with the lowest freezing points. It is also worth noting that the sample at the surface at 30cm has almost no chloride content at all, most likely due to the distance between the sample and the sea ice.

From figure 4.11, the correlation between NO_3^- and the samples freezing temperatures can be observed. In general, all of the samples contain a very similar NO_3^- content apart from the sample at 18cm which conveys a strong relationship with NO_3^- and holds the highest nitrate content of any of the samples. This amount of nitrate appears to have caused a significant freezing point depression,

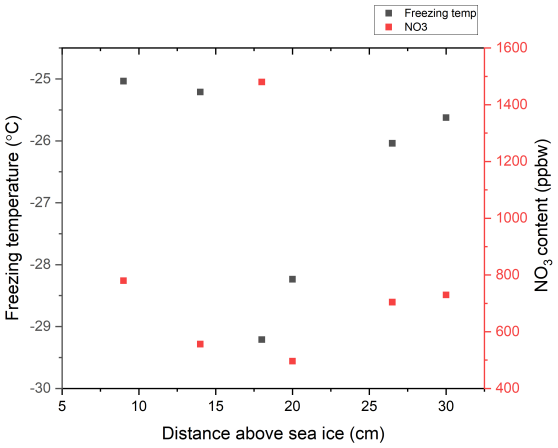

Figure 4.11: The nitrate content of each sample displayed alongside their freezing temperature and distance above the sea ice

conveying that the sample at 18cm (0839) was not pure at all and instead contaminated with NO_3^- however, similarly to the chloride, the amount of depression expected from a salt is less than a degree centigrade making it more likely to be a correlation rather than causation. All of the other samples demonstrate a similar relationship, with the higher the NO_3^- the greater the temperature depression apart from the sample at 5cm which, as with the Cl content, would be expected to have a lower freezing temperature for the amount of NO_3^- it contains if the effect of freezing point depression was more significant.

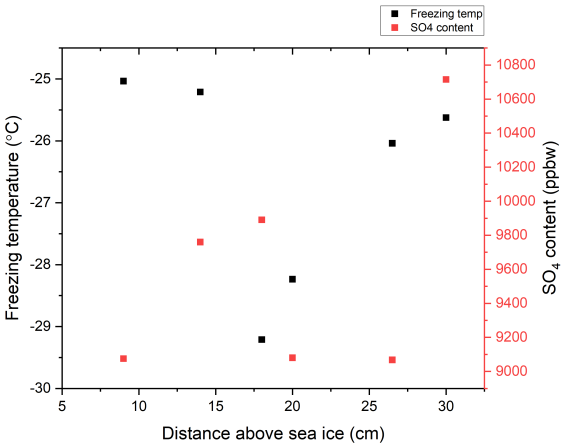

Figure 4.12: The sulphate content of each sample displayed alongside their freezing temperature and distance above the sea ice

The sulphate content found in each sample is portrayed in figure 4.12. As a salt, this should also cause a minimal freezing point depression in the samples however, the sample at 30cm (the one found

on the surface of refrozen lead) has the highest sulphate content whilst still experiencing quite a high freezing point. Interestingly, this indicates that there are also separate INPs influencing the surface sample. The only sample seeming to be affected by $SO_4{}^{2-}$ is once again the sample at 18cm although the sulphate content for all the samples are actually insignificantly different. Overall, it is unlikely that the Sulphate is having any impact on the freezing temperature. Sea water has an average sulphate content of 2 million parts per billion weight, so that fact that every sample is within the range of 10,000ppbw shows that most likely, it is not having an effect.

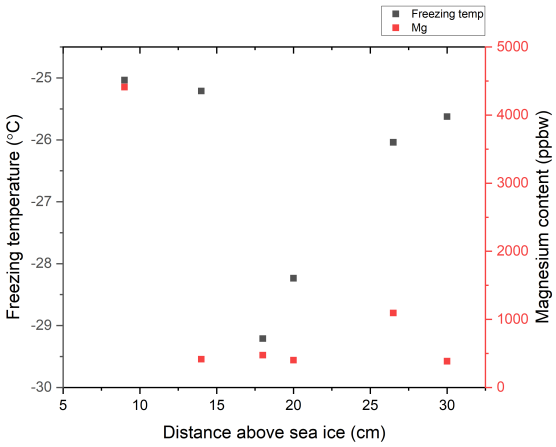

Figure 4.13: The magnesium content of each sample displayed alongside their freezing temperature and distance above the sea ice

In this last figure 4.13, the magnesium content in each sample is shown. The magnesium content specifically is not a relevant factor as it would most likely be present in the form of a chloride or sulphate salt which have already been discussed, however it demonstrates that apart from the salts, the sample at 5cm measured very highly for every other ion. This includes oxalate, ammonium and other single elements such as potassium and calcium. None of the other samples display this quantity of ions and this is likely due to the proximity of the sample to the sea ice.

4.4 Discussion

Given the results from the previous section it appears that each sample has a unique mixture of ions and INPs affecting the freezing point. This is to be expected since they were taken from different heights in the snow however the chloride salt did not permeate as much as was expected and actually made little difference to the freezing point of the samples. Since seawater has its salinity reduced when it freezes into sea ice due to brine rejection, it is possible that more of an effect would have been seen if pure sea water samples had been used. For the purpose of this experiment however, it is very interesting to see that even when snow is so close to the sea ice, the salt itself is not the main influence over its freezing temperature. The sample closest to the sea ice was 0666 at 5cm. As this sample experienced very high

values for every ion including Calcium, Potassium and Magnesium which are regularly found in sea water, it seems that its freezing temperature must have been increased by a species that was not measured however was present in the sea water itself. It is possible that this increase in ice nucleating ability was caused by an organic INP such as a diatom [46] or heat labile biological materials such as phytoplankton [47]. Irish *et al* [47] found a strong correlation between the salinity of the seawater and the abundance of bacteria present when investigating in the Canadian Arctic. For the sample at 5cm, which displayed the highest chloride content yet still had the highest freezing point, this would provide an interesting perspective. As Carbon content was not measured, it is difficult to know whether biological material was present in the sample. It seems most likely that biological INPs are the cause of this high freezing point however Irish *et al* also go on to claim that the size of the INPs in their study were under 0.2μm. This would imply that the INPs are exudates from phytoplankton or bacteria or potentially species such as viruses and ultramicrobacteria instead. This is definitely still a possibility for the samples used in this project and would supply an explanation for why the freezing point did not match with any existing trends for the ions measured. Another potentially interesting point for this sample is the fact it was collected in the presence of a film crew and had the smallest distance between it and the transponder. Whether this would have had an effect on its collection environment is unlikely given its depth in the snow but is worth nothing nevertheless.

Sample 0774 at 14cm is the second closest to the sea ice but does not present high contents of any ion apart from sulphate. It also has a high freezing point and since sulphates only cause a negligible freezing point depression, it is clear that it may be biological factors affecting this sample. In a paper by Worthy *et al* [48] they highlight the effect of ammonium sulphate on the ice nucleating ability of biological INPs. They found that the presence of $(NH_4)_2SO_4$ had no effect on the freezing temperature of samples containing INPs such as diatoms, exudates and bacteria. This implies that even under the influence of a high salt content which would normally lead to a freezing point depression, biological INPs can nullify the effect and still raise the samples freezing point. This is interesting as it means that the INPs could help initiate freezing in the Artcic at higher temperatures which would be useful given the rate of melting sea ice. This sample is most likely to experience the effects of INPs from upwards migration from the sea ice.

With the lowest freezing point of any of the samples, 0839 at 18cm has very high contents of NO_3^- and $SO_4{}^{2-}$. Both of these, as salts, cause a small freezing point depression as already discussed which could explain why the freezing point is so low however it is more likely to be caused by a lack of INPs. The salt content it does have (ammonium and sulphate) are not in a high enough quantity to reduce the freezing point significantly however it is still uncertain where their presence originated from. As 0839 does not contain a high content of chloride, it can be assumed that the other salts did not come from upwards migration. If they had, it would be expected that the samples below at 5 and 14cm would have an NO_3^- content as high, if not higher, than the sample at 18cm. This is not the case, with sample 0839 experiencing a nitrate count double that of any other sample. It is potentially caused by deposition from the atmosphere but as this is not a surface sample and the average snow depth for February (when this

sample was collected) is 29.7cm [49], the contaminants would have had to be present in the snow during precipitation.

The sample with the least contamination is 0656 at 20cm above the sea ice. It contains very low amounts of every single ion, including oxalate and chloride. Given the information provided, it appears that this sample is the cleanest overall and this may explain it's relatively low freezing point as there are likely very few INPs present. It is the closest example of a pure sample, with little to no content of any ion that would cause either freezing point depression or increase its ice nucleating ability. As it is 20cm above the sea ice, it is safe to assume that upwards migration has not affected it considerably, explaining its very low salt content. It is also deep enough so that atmospheric conditions such as pollution etc has not been able to reach it. Interestingly, this sample was collected in the same place at exactly the same time as sample 0774 in January. This sample also had very low ion contents but experienced a higher freezing temperature probably due to its proximity to the sea ice. It is intriguing that both of these samples had the smallest quantity of measured ions and they were both collected in the same place. Further information on their collection was not provided however it would be a valuable topic to investigate.

At surface level, sample 0036 has quite a high freezing point at -25.94°C. It was located furthest away from the sea ice however still contains salt contents that are relatively high. Although it does not appear so on figure 4.10, this sample has a chloride content of 16694ppbw which, compared to the sample closest to the sea ice, is quite low however every other sample has a content in the low thousands if not hundreds of parts per billion weight. This is most likely caused by sea spray however this sample appears not to be experiencing a freezing point depression. Similarly to the earlier samples that were also in contact with the sea water, the freezing point depression has likely been counteracted with biological INPs, increasing the freezing point of the sample.

The last sample was collected from refrozen lead as freshly fallen snow. It contains the highest sulphate content of any sample however this appears not to be the result of sea water contamination since the chloride content recorded is very low. Compared to the sample at sea ice level, this sample has a sodium content 800 times lower at only 50.7ppbw. Given this fact, it is most likely that the sulphate is present due to atmospheric pollution rather than from the sea water. This still does not explain its high freezing point however as sulphate would cause a freezing point depression if it had any effect at all which it is unlikely to do given the quantity present. To cause a higher freezing point, other elements such as mineral dust INPs are probably the cause creating an increase in ice nucleating ability. There are many atmospheric INPs (including biological aerosols such as fungal spores and bacteria) which present a reasonable explanation as to this sample's higher freezing point. As well as this, sample 1476 was collected from a lead in an area known as Met City, the meteorological research area on an ice floe, created alongside several other research camps and the RV Polarstern itself. Whether this location would affect the result due to an increased population in its vicinity is theoretically possible but with the data provided it is difficult to know for certain. Having the Polarstern and a runway nearby is likely to have increased the pollution in the area which may provide an explanation for the high freezing point

experienced even though the snow had only recently fallen.

Experimentally, the results obtained are precise as, due to the repeat measurements, anomalous results could be removed from averages. The anomalies could have been caused by the formation of condensation in the cold stage. This occurred when the cold stage was not given enough time to warm up between runs, producing condensation on the glass screen. This did not affect the actual freezing point of the droplets however it made the analysis more difficult. As the freezing point was determined using a python detection system, when condensation interfered it could not properly locate the time at which freezing occured forcing a manual determination. This meant that results were not as accurate or reliable as computer detection. To avoid this, nitrogen gas could be pumped into the cold stage in between experiments. It is not feasible to routinely wait for the stage to completely warm up however an alternative would be to create a heating ramp to speed up the process. This would be easy to achieve using the Peltier cooler and could be done as a stand alone practice or before the nitrogen gas is introduced. To determine the presence of biological INPs, the samples could be dry heated at 250°C before being tested again. This would deactivate all of the biological INPs and give a clear indication of whether it was their presence affecting the results in the first measurements [50].

4.5 Conclusions

In conclusion, the salt content present in these Arctic snow samples seem to have had a minimal effect if any. Due to the relatively low concentration, a freezing point depression could not be identified as a significant factor to any of the samples freezing points. The sample with the least INPs present appeared to be sample 0839 at 18cm which makes sense as it is situated almost centrally between the sea ice and the atmosphere making the amount of contamination it receives as low as possible. This is reflected in its very low freezing point. For all of the samples with a high freezing point, it is most likely biological particles such as ultramicrobacteria or exudates from phytoplankton that have caused the raise. To gain a better insight into this, the samples could also be tested for carbon content. In wider terms, this project highlights the importance of thoroughly documenting where and when samples are collected as the environment they are taken from has the possibility of hugely impacting the results, as seen in the sample taken from MetCity.

CHAPTER 5

NUCLEATING ABILITY OF THE HGD ENZYME

5.1 Introduction

Homogentisate 1,2-dioxygenase (HGD) is an enzyme primarily found in the liver and kidneys of humans and contributes to the breakdown of amino acids tyrosine and phenylalanine [51]. It is created by a gene of the same name that codes for the enzyme consisting of 445 amino acids. HGD itself has a hexameric structure, meaning it contains six molecules of the same monomer, arranged as a dimer of two trimers [52]. In figure 5.1 below a prediction of the fold structure of the HGD enzyme can be seen, created on AlphaFold.

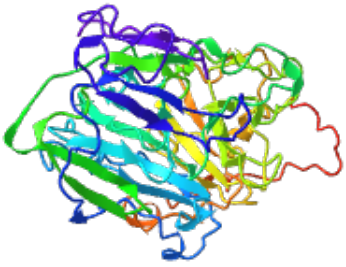

Figure 5.1: AlphaFold prediction of the structure of HGD [5] [6]

If the body is deficient in HGD, a condition called Alkaptonuria is developed resulting from increased levels of homogentisic acid (HGA). This acid is a product of the metabolism of tyrosine and becomes harmful when HGD is unable to split the HGA aromatic ring [53]. When levels increase, the urine and ear wax of patients turns black due to its oxidation into a melanin type polymer. This can then spread further and presents as black tissue in the eyes and if untreated causes degeneration in the joints [54].

This project however, focuses on the ice nucleating ability of the HGD enzyme rather than its medical effects. By investigating the behaviour of HGD during freezing, it can be established whether the enzyme acts as an ice nucleating agent or as an antifreeze protein. This is vital information pertaining to the cryopreservation of organs as the effect of enzymes on ice formation is unknown. The analysis of HGD therefore acts as a representative for other enzymes too. According to the World Health Organization only 10% of the demand for organ transplants was met in 2010[55] with two thirds of heart donations[56] and 20% of kidney donations simply discarded[57]. This is due to the amount of time that organ donations can be stored for and is a serious problem worldwide. To combat this, improvements in cryopreservation are required that allow organs to be stored safely for much longer durations until a recipient can be found, reducing waste and providing more people with life saving transplants. Acting as either an INP or an antifreeze protein would affect the cryopreservation process in enabling the storage of the kidney in the most effective condition. During the cooling process, it is common practice to mix the cells or tissues with a cryoprotective agent (CPA)[58]. Some of these CPAs are antifreeze proteins which protect cells from cryoinjury by regulating rates of nucleation, ice crystal growth and water transport. If HGD itself acts as an antifreeze protein, the cryopreservation cooling rate would have to be increased slightly or it will result in cryoinjury [58]. Due to the osmotic changes caused by the high concentration of intracellular solutions and CPAs, the cell is sometimes unable to transport water out of its cell membrane causing intracellular freezing [59]. In this way, it is vital to understand the freezing behaviour of HGD so that it can be handled in cyropreservation accordingly.

In this section of the thesis, the experimental details of the HGD measurements are presented from the sample prepraration to the experimentation itself. To investigate the freezing behaviour, samples of HGD were cooled, both linearly to observe the temperature at which 50% of the droplets had frozen and isothermally. Samples of pure buffer as well as a sample made from 50% HGD solution and 50% pure buffer were also experimented on to help draw an accurate conclusion on the HGDs freezing rate. During the experimentation, obstacles such as the age of the sample were met and a full discussion into the limitations of the experiment are presented at the end of the chapter. With all the information provided, a conclusion will be given on the behaviour of the HGD and to which class, either INP or antifreeze protein, it belongs to.

5.2 Experimental Methods

5.2.1 The Sample

The sample of Homogentisate 1,2-dioxygenase used in this project was produced by Ellen Carrick as 5mg of HGD in 0.275M Sodium Acetate at a pH of 4.5. This equated to an HGD concentration of 1.47mg/ml. The gel electrophoresis seen in figure 5.2 shows the molecular weight of the sample to be 20kDa however beta-mercaptoethanol was added to prevent the formation of dimers which the hexameric structure of HGD relies on. Therefore, the real molecular weight of the sample is around 40kDa.

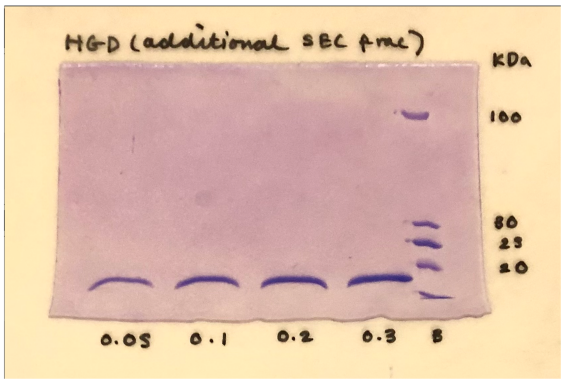

Figure 5.2: A gel electrophoresis measurement for the HGD sample taken by Ellen Carrick

5.2.1.1 Silicon substrate preparation

The procedure discussed in this section was developed by Sarah Alsalhi

For every experiment conducted with the HGD, the sample was pipetted onto specially prepared silicon substrates around 1cm by 1cm in size. To make these, a silicon wafer was used. Starting from the straight edge (as this indicates the (110) orientation) a scriber was pressed firmly against the edge to split the wafer. This uses the crystal planes of the silicon wafer to split it evenly without uneven breakages. This was done as many times as necessary to produce as many substrates of the correct size as possible (around 40 per wafer). Once they were cut, the substrates were placed into a beaker with some washing up liquid and filled with MilliQ water. The beaker was then placed into an ultrasonic bath and sonicated for 15 minutes to clean the substrates.

When the sonication was finished, the substrates were rinsed thoroughly with MilliQ water and, when it was clear there was no soap left (there was no foaming present), they were placed into a beaker containing 100ml of MilliQ water. To this, 500μl of DMOAP (Dimethyloctadecyl[3-(trimethoxysilyl)propyl]ammonium chloride) was pipetted into the solution under the fumehood. This was done as DMOAP creates a hy-

drophobic coating on the substrate to prevent the droplets smearing and merging into one another. It also makes contamination of the sample less likely. The whole beaker was then shaken by hand for 5-10 minutes to ensure the substrates were properly coated with the solution. After this, they were again thoroughly rinsed with MilliQ water to remove the DMOAP, then individually dried using Nitrogen gas and placed into a glass saucer covered in foil. They were then baked for an hour at 120°C.

5.2.2 Linkam Cold Stage

For both the frozen fraction and isothermal measurements at the University of Bristol a Linkam THMS600 was used to acquire results. It differed from the one used at BAS as it used liquid nitrogen to cool rather than a peltier cooler and water pump. The liquid nitrogen was directly injected into the silver cooling stage and did not require initial cooling to a start temperature as the water pump did.

Firstly, the substrate and sample were prepared. Although initially coated with DMOAP, the silicon substrates were treated with a second hydrophobic coating before they were used experimentally. They were rinsed with MilliQ and dried using Nitrogen gas before being placed in a container of 'Nano Tech Speed Guard', a hydrophobic solution used to protect cars. It created a nano hydrophobic coating which ensured that the droplets would remain the correct shape and that the substrates would repel dust as much as possible. After sitting in the solution for about 5 minutes, the substrates were rinsed with MilliQ water again and then again dried with Nitrogen gas.

Once the substrate was ready, the dewar was filled with liquid nitrogen and connected to the cold stage. As the sample needed to be refrigerated, pipetting it was the last thing to be done to reduce the amount of time out of the fridge. The sample was pipetted as μl droplets onto the silicon substrate with positions judged by eye so droplet arrangements were not as regular as the droplets from BAS. The silicon substrate and sample were then placed onto the cold stage and the lid was screwed on. The LED ring of lights was then attached to the top of the cold stage using velcro and then the whole setup was placed under the microscope and the specially designed screen to prevent the light escaping. The reflected light gave very clear images of the droplets and increased clarity when recording freezing.

To conduct the experiments, the equipment was first turned on to begin loading the software on the computer. The software used for these experiments was MoticPlus for the imaging, connected to the camera on the microscope, and LINK temperature controller. Due to the processing time, images were taken every 5 seconds. Any more frequently than this would cause too many images to be recorded and the computer would crash. For linear cooling, two ramps were used to speed up the data collection. The first ramp was 30°C/min until -20°C and the second was 1°C/min until -32°C or all of the droplets were frozen. The camera started recording images at the start of the second ramp. The temperature of -20°C was chosen as it was observed that was around the temperature that the first droplets froze. For isothermal measurements, it was observed from linear cooling measurements that the majority of droplets froze around -24°C so experiments were run from -22 to -28°C. A cooling ramp was used again except this time it was 30°C/min until the target temperature and then it was held with a 'ramp' of 0°C/min for 1800 seconds. This would hold the sample at the target temperature for half an hour and

that was the duration that images would be taken for. Results were recorded for temperatures -22, -24, -25, -26 and -28°C. The images were then analysed using ImageJ with the slice number translating to a time and hence temperature.

5.2.3 Dynamic Light Scattering

To establish what was present in the HGD solution (to aid in the analysis of the freezing results), dynamic light scattering was performed on the sample. Around 2ml of the HGD protein (suspended in a Sodium Acetate buffer) was syringed into a glass vial. The vial had previously been washed with the buffer. The laser was then prepared. The detector was set to record at the 637nm setting and the laser was uncovered. To ensure the setup was operating correctly a Latex control sample was used which should give a single line on the detected intensity. When this was observed, the latex was replaced with the sample tube. On the software, the parameter for refractive index was set to water given that the actual refractive index was unknown and the device was turned on. The results were recorded as excel data.

5.3 Results

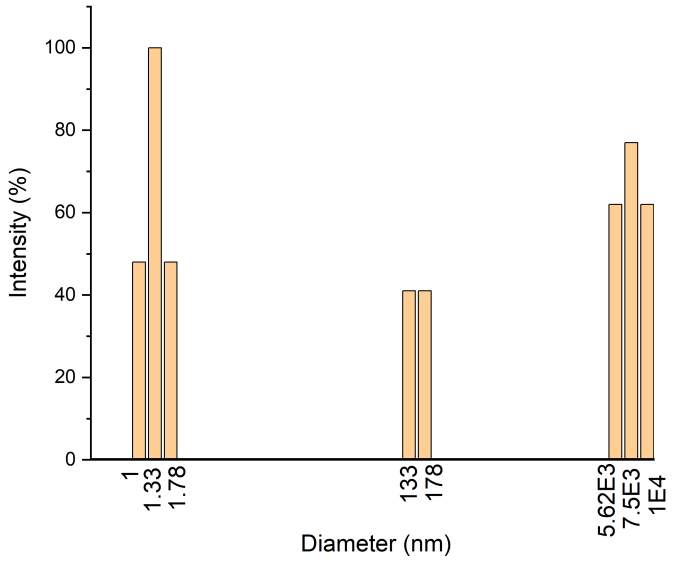

Figure 5.3: A graph showing results from the DLS indicating the size of particles located in the sample

The results can be seen in figure 5.3 where there appears to be three separate regions of interest with varying diameters. Since the enzyme has a molecular weight of 20kDa (or 40kDa in its proper hexameric form), it is estimated that its diameter will range somewhere between 1 and 4nm [60]. From figure 5.3, the first set of three intensities is therefore most likely to be caused by the enzyme. For 20kDa, 1.78nm is an expected diameter for a protein however for 40kDa all of the first set of values are a little small.

The middle set is almost certain to be caused by aggregation of the protein in the solution. The third and final set of intensities are considerably larger in diameter and are likely to be the product of dust particles that have fallen into the solution. Due to the way samples are decanted, it is difficult to remove all dust and it can be assumed a similar presence would be found in the buffer solution. Therefore, the difference between the sample and the buffer are most likely to be caused by the enzyme rather than dust which is expected to be present in both.

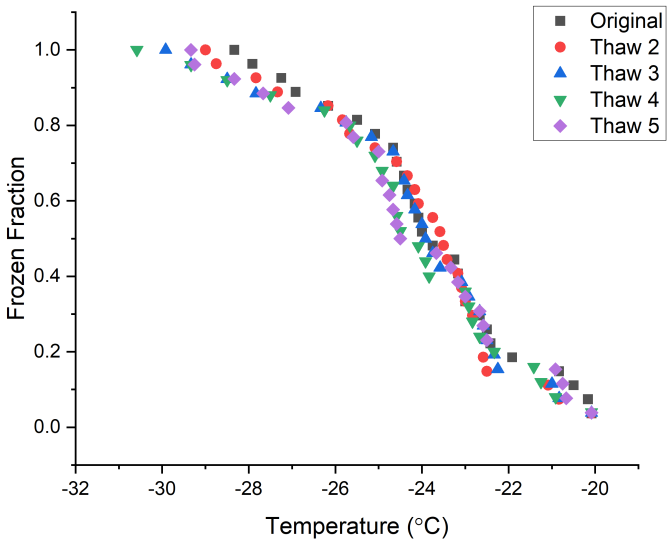

Figure 5.4: A graph showing multiple freeze-thaw runs for the HGD sample

To commence this section of the project, the HGD sample was first tested for its resistance to being frozen and thawed multiple times. If the same sample was capable of being repeatedly experimented on, it would save time and the volume of HGD required for testing. Figure 5.4 demonstrates the frozen fraction for a sample of HGD after having been frozen and thawed 5 times. The first thaw sample was not properly recorded by the camera so the experiment continues from the second thaw onwards. The results show, regardless of the missing data set, that the HGD is able to be frozen and thawed multiple times without effect on the freezing behaviour as each run has an almost identical curve. This demonstrates that for this sample, the enzyme itself is unaffected by freezing. With this information, it was safe to assume that the same sample could be used for multiple runs at different temperatures.

After this, it was important to investigate whether the HGD sample was providing a different result than the pure buffer. As the HGD was in a solution of Sodium Acetate, it would have been possible that only the buffer was demonstrating ice nucleating effects. Figure 5.5 however shows a clear distinction between the HGD sample (coloured runs) and the buffer (black runs). At 50% frozen fraction, the buffer had an average freezing temperature almost 2 degrees lower than that of the HGD. This was evidence that the enzyme was having an impact on the ice nucleating ability of the sample.

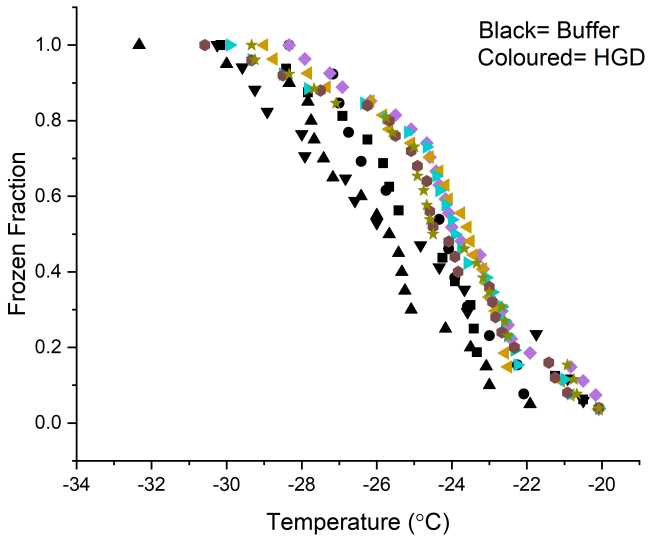

Figure 5.5: A graph showing a comparison between HGD freeze-thaw runs and the buffer

For the rest of the results, isothermal measurements were more suitable than frozen fraction as they better demonstrate the ice nucleating effects acting on the sample. Both the HGD and buffer isothermal curves can be seen in figures 5.6 and 5.7 respectively. The HGD sample shows a much steeper curve for every temperature, except where the sample was held at -22°C and this appears to be too high of a temperature for a significant number of droplets to freeze. The run at -24°C was cut short due to a malfunctioning of the camera however its initial curve shows its trajectory was steeper than the buffers. Figure 5.6, as well as the frozen fraction curves before it, indicate that the HGD acts as an ice nucleator, increasing the required freezing temperature. These graphs also show the ideal temperatures for isothermal experiments to best compare the HGD samples to the buffer. The highest temperature (-22°C) was not cold enough to provide sufficient data and the lowest temperatures (-26°C and -28°C) were very steep curves which are unideal due to their ability to be affected by non-uniform temperature distributions within the droplet. When the sample cools too quickly, it is likely that a uniform temperature has not had a chance to establish within the droplet creating inaccurate results. In this example however, the curves at -24°C and -25°C exhibit a two step freezing pattern. An explanation into why this occurs will appear in the discussion, however it meant that these temperatures were not ideal to use given the multiple factors affecting the results. For this reason, the lowest temperatures were chosen to compare between HGD and the buffer solution as the immediate freezing behaviour could be isolated and analysed.

To compare the isothermal behaviour of the HGD enzyme to the buffer, curves at -26°C and -28°C were plotted together on figure 5.8. Results for a 50% HGD and 50% buffer solution (denoted 50/50) were also plotted. The 50/50 solution has an HGD concentration of 0.74mg/ml and enables a test of

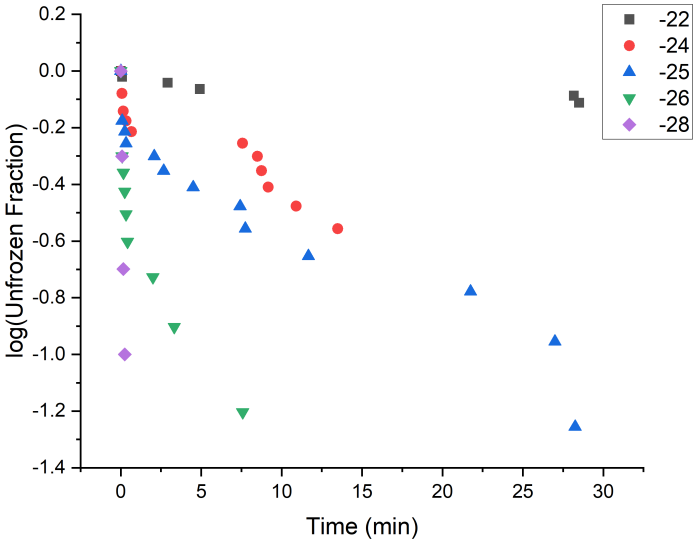

Figure 5.6: Isothermal results for the HGD sample at 5 different temperatures

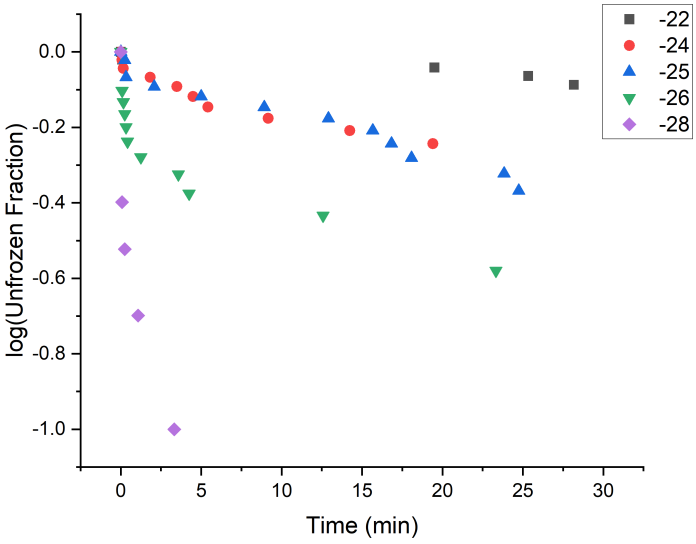

Figure 5.7: Isothermal results for the buffer at 5 different temperatures

whether the sample at half concentration would provide an isothermal curve with half the rate of freezing. Ideally, this curve would sit between the protein and buffer curves. Figure 5.8 however shows that the 50/50 solution had a slower freezing rate than the buffer. To test whether this was due to the age of the protein, another run was carried out for the 50/50 solution. The results can be seen in figure 5.9 together

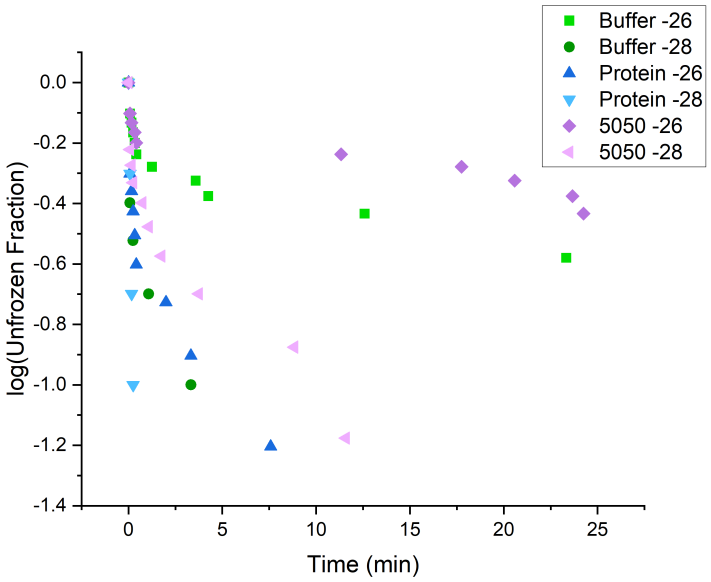

Figure 5.8: A graph comparing the isothermal results from the HGD, buffer and the 50/50 solution taken on the 27th of May

with the protein and buffer data from figure 5.8. In this graph, the lower concentration HGD solution had a very slow freezing rate at every temperature, with the curve at -28°C slowing by 25%. For this reason, the last figure should be disregarded as the lower concentration solution is clearly no longer under the influence of the enzyme.

5.4 Discussion

From the results in the previous section, it can be concluded that Homogentisate 1,2-dioxygenase behaves as an ice nucleator rather than as an anti-freeze protein. It experienced a faster rate of freezing, at lower temperatures, for both the linearly cooled and isothermal experiments.

Interestingly, the two step freezing pattern seen in figure 5.6 seems to have been caused by frost formation. Figure 5.10 shows a snapshot of the end of the isothermal run at -24°C and demonstrates the frost that had formed around the droplets. The frost stretches out and makes contact with other droplets around it causing a second 'wave' of freezing. The areas where frost has made contact can be seen in figure 5.10 and are highlighted with red circles.

The formation of frost in the form of these dendritic branches can be explained using the thermodynamics associated with ice growth. The equation for free energy ($\Delta G = \Delta H - T\Delta S$) contains a term for enthalpy (H), temperature (T) and entropy (S). When the sample is a liquid, the enthalpy and entropy terms are higher than for a solid. When ice forms, the entropy is reduced as it adopts a more structured configuration. This decreases the free energy and makes freezing a more favourable interaction below

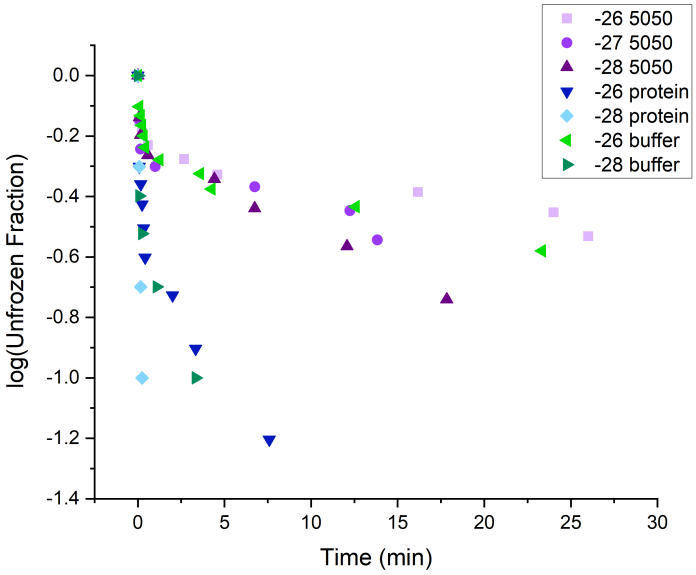

Figure 5.9: A graph comparing the isothermal results from the HGD, buffer and the 50/50 solution taken on the 14th of June

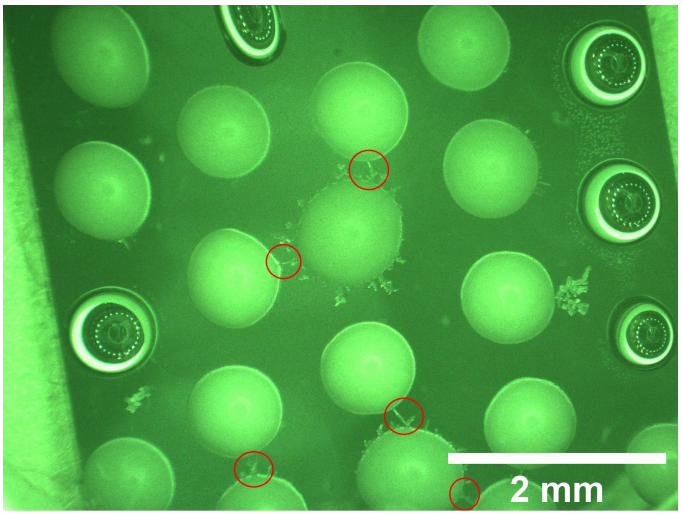

Figure 5.10: A photo of the HGD droplets during the isothermal run at -24°C. The red circles highlight where the frost formation has made contact with other droplets

0°C. As the entropy is reduced in the sample, energy is forced to escape to the surroundings resulting in an increase in temperature. The amount of latent heat produced by freezing is too great to be absorbed by the water itself. This causes the frozen droplet to heat up to a maximum of 0°C as the freezing is limited by the rate of the release of latent heat of fusion. To reduce its temperature it has to remove heat faster and the formation of dendrites achieves this. During the release of heat, an instability (called the

Mullins-Sekerka instability) causes a protrusion to form on the droplet. This protrusion compresses isotherms of the latent heat field causing it to experience a larger temperature gradient resulting in increased heat flow away from the droplet. The protuberance then grows faster creating longer dendrites [61]. To reduce the presence of these, a slower cooling rate could be used. This would allow the droplet more time to release the heat and remove the necessity for dendrite growth. Alternatively, the same effect would be achieved by increasing the humidity in the stage as the heat would be unable to evaporate as quickly, reducing the cooling rate. By slowing the cooling rate however, not only is the process more time consuming and computationally expensive but it also increases the probability of freezing which could alter the results unintentionally.

The most interesting factor in this frost formation is that it is not very noticeable for the buffer. It appears on the images but the trend is difficult to locate on the graphs. This may be due to the results being taken two days apart with differing temperatures or it could be due to the slower rate of freezing experienced by the buffer. If left longer, a second 'wave' of freezing may have occured. It is also possible the droplets were just positioned further apart than the HGD sample droplets. In figure 5.11 the frost formation for the buffer can be seen as well as a condensation vapour on the glass. Finding the average temperature on the days these experiments were conducted [62] shows that the dew point on the day of the buffer experiment was 3 degrees higher than for the HGD experiment. When the surface temperature is below the dew point it is likely that vapour condensation will form and then freeze once the surface temperature goes below 0°C [63]. This seems to be what has happened in this case. The condensation is more likely to have formed for the buffer and not the HGD as there was a greater temperature difference between the surface and the dew point however is unlikely to be the reason why a two step pattern was not identified.

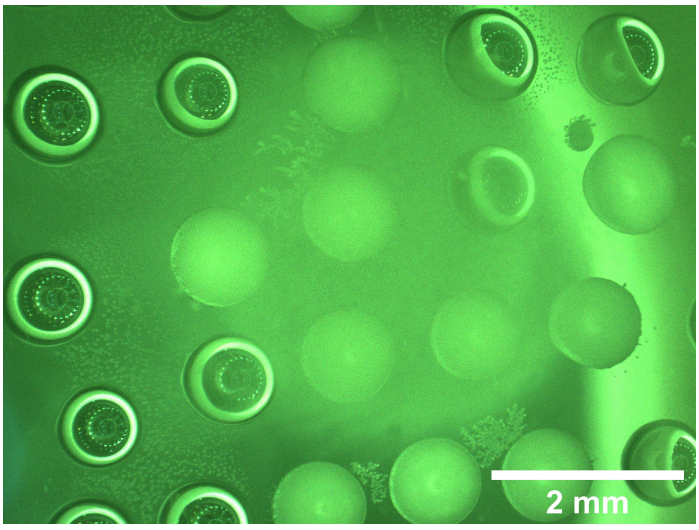

Figure 5.11: A photo of the buffer droplets in an isothermal experiment at -24°C. There is the presence of frost and a frozen condensation vapour

Although figures 5.8 and 5.9 did not demonstrate lower freezing rates for the lower concentration of

HGD, it did demonstrate the aging of the protein. The frozen fraction results were taken in late March, the HGD and buffer isothermals in early May and the 50/50 solution was tested in late May (figure 5.8) and mid June (figure 5.9). As the sample was stored in a pH 4.5 buffer in a fridge (around 5°C), it's lifetime is predicted to be several weeks at most. The sample had begun to show signs of denaturing during the isothermal tests however it was re-filtered, put into the centrifuge and the results seemed to stabilise again. By the time of making the 50/50 solution, it can be observed from the figures that the sample was displaying more similar behaviour to the buffer than that of the enzyme. In the second graph two weeks later, the enzyme shows a complete loss of ice nucleating ability and behaves most similarly to the buffer at it's highest temperature. In both of these examples it is also possible (especially at lower temperatures) that the freezing was a mixture of enzyme and buffer induced freezing which, as the protein denatured, was dominated by the buffer. Fortunately the comparison between the original HGD and buffer samples displays the successful ice nucleating ability of the enzyme.

5.5 Conclusion

In summary, the HGD protein acts as an ice nucletor rather than as an anti-freeze protein. It encourages freezing at higher temperatures and froze significantly faster than the buffer alone. It is likely to have formed aggregates and experienced a two-step freezing pattern due to the formation of dendrites growing and making contact with other droplets. This topic would benefit from further research. It would be useful to conduct another DLS measurement and to test another HGD sample at varying concentrations to firmly establish its behaviour as an ice nucleator.

CHAPTER 6

SUMMARY

This thesis was split into three independent research projects with different aims. In the first project, the ALTA was adapted to create a piece of equipment that could observe freezing for multiple droplets. It also lends itself to incorporation with microfluidics. The second project involved an investigation of six Arctic snow samples to test the affects of salinity on the freezing temperature of snow and hence, seawater. For the final project, the behaviour of Homogentisate-1,2-dioxygenase was explored to establish whether it acted as an ice nucleator or an anti-freeze protein.

From Chapter 3, the ALTA was successfully developed to achieve temperatures as low as -22.4°C in just over a minute and -28.7°C in ten. By using a thermal paste commonly found in computers (MX4), an effective connection could be made between the Peltier cooler and the sample. This ensured that the sample could get as cold as possible as fast as possible. With the new flat surface design, microfluidics are now able to be included so that many, smaller droplets can be used in experiments providing larger statistically valuable data sets. Edits still need to be made to the software to optimise the operation of the experiments however the equipment showed potential for future projects or for use in the teaching labs.

The data collected at the British Antarctic Survey, discussed in Chapter 4, demonstrated that salinity had a minimal effect on the freezing temperature of seawater samples. The concentration of salts found were too low to exhibit a freezing point depression of any significance and could not prove the impact of salinity. Samples 0839 and 0656, located in the centre of the sea ice, experienced the lowest concentration of all INPs and hence, the lowest freezing points. They were unaffected by the contamination of salts from the sea or from atmospheric particles. Where the freezing point was affected, it was most likely caused by biological particles such as ultramicrobacteria or exudates from phytoplankton which would act as INPs. Most of the recorded INP concentrations did not align with the freezing points experienced by the samples. To ascertain whether organic material could have been the cause of higher freezing points, it would be beneficial to test the samples for their Carbon content.

In the final chapter, HGD was found to act as an ice nucleator rather than as an anti-freeze protein demonstrated by it freezing at a higher temperature than the buffer sample. It displayed a faster freezing rate in both linear and isothermal experiments. DLS results showed this may be partly due to aggregates however the rate was also increased by the formation of dendritic branches. Further research would be useful to test the effect of HGD at different concentrations and to re-evaluate the aggregation that occurs in the protein using DLS and gel electrophoresis. These results may help researchers understand how enzymes affect ice formation which will be very valuable in the context of cryopreservation.

BIBLIOGRAPHY

[1] Axel Seifert, Carmen Köhler, Claudia Fricke, and Heini Wernli.
Cloud microphysics in the cosmo model: New parameterizations of ice nucleation and melting of snow.
COSMO General Meeting, WG3-Session, 2009.

[2] Christian Eberhard.
Dissertation on the development of a model system to study cell adhesion and cell mechanics (image used).
Ruperto-Carola University of Heidelberg, 2012.

[3] B. Vonnegut and M. Baldwin.
Repeated nucleation of a supercooled water sample that contains silver iodide particles.
Journal of Climate and Applied Meteorology, 23(3):486–490, 1984.

[4] Fred Cook.
Development of apparatus for ice nucleation studies, (thesis).
University of Bristol, pages 5–42, 2020.

[5] J. Jumper et al.
Highly accurate protein structure prediction with alphafold (image used).
Nature, 596:583–589, 2021.

[6] M Varadi et al.
Alphafold protein structure database: massively expanding the structural coverage of protein-sequence space with high-accuracy models (image used).
Nucleic Acids Res., 50(D1):439–444, 2021.

[7] George Wypych.
Handbook of Nucleating Agents.
ChemTec Publishing, 2016.

[8] Gabriele C Sosso, Ji Chen, Stephen J. Cox, Martin Fitzner, Philipp Pedevilla, Andrea Zen, and Angelos Michaelides.

Crystal nucleation in liquids: Open questions and future challenges in molecular dynamics simulations.
Chemical Reviews, 116(12):7078–7116, 2016.

[9] G. John Morris and E. Acton.
Controlled ice nucleation in cryopreservation - a review.
Cryobiology, 66(2):85–92.

[10] James D. Atkinson, Benjamin J. Murray, and Daniel O Sullivan.
Rate of homogenous nucleation of ice in supercooled water.
J. Phys. Chem. A, 120(33):6513–6520.

[11] M. Nicolaus et al.
Overview of the mosaic expedition: Snow and sea ice.
Elem Sci Anth, 10(1):1, 2022.

[12] K.F. Felton.
Nucleation.
Encyclopedia of Materials: Science and Technology, pages 6388–6392, 2001.

[13] Holden et al.
Active sites for ice nucleation differ depending on nucleation mode.
PNAS, 118(18), 2021.

[14] J. Atkinson, B. Murray, and M Woodhouse et al.
The importance of feldspar for ice nucleation by mineral dust in mixed-phase clouds.
Nature, 498(7454):355– 358, 2013.

[15] Viviane R Després et al.
Primary biological aerosol particles in the atmosphere: a review.
Tellus B: Chemical and Physical Meteorology, 64(1), 2012.

[16] Gregory P. Schill and Margaret A. Tolbert.
Heterogeneous ice nucleation on simulated sea-spray aerosol using raman microscopy.
The Journal of Physical Chemistry C, 118(50):29234–29241, 2014.

[17] Sarah D. Brooks, Katie Suter, and Laura Olivarez.
Effects of chemical aging on the ice nucleation activity of soot and polycyclic aromatic hydrocarbon aerosols.
J. Phys. Chem. A, 118(43):10036–47, 2014.

[18] H. R. Pruppacher and J. D. Klett.
Microphysics of clouds and precipitation.
Kluwer, Dordrecht, 1997.

[19] B. Zuberi, A. K. Bertram, T. Koop, L. T. Molina, and M. J. Molina.
Heterogeneous freezing of aqueous particles induced by crystallized $(NH_4)_2SO_4$, ice, and letovicite.
J. Phys. Chem. A, 105(26):6458–6464, 2001.

[20] Hoose et al.
A classical-theory-based parameterization of heterogeneous ice nucleation by mineral dust, soot, and biological particles in a global climate model.
Journal of the Atmospheric Sciences, 67(8):2483–2503, 2010.

[21] R. Jaenicke, S. Matthias-Maser, and S. Gruber.
Omnipresence of biological material in the atmosphere.
Environ. Chem, 4:217–220, 2007.

[22] Richard E. Lee and Jon P. Costanzo.
Biological ice nucleation and ice distribution in cold-hardy ectothermic animals.
Annual Review of Physiology, 60:55–72, 1998.

[23] John G. Duman.
Antifreeze and ice nucleator proteins in terrestrial arthropods.
Annu. Rev. Physiol, 63:327–57, 2001.

[24] R. J. Bodnar.
Revised equation and table for determining the freezing point depression of H_2O-NaCl solutions.
Geochimica Et Cosmochimica Acta, 57(3):683–684, 1993.

[25] Mark C. Serreze, Marika M. Holland, and Julienne Stroeve.
Perspectives on the arctic's shrinking sea-ice cover.
Science, 315(5818):1533–1536, 2007.

[26] David Richard and Thomas Speck.
Classical nucleation theory for the crystallization kinetics in sheared liquids.
Phys. Rev. E, 99(6):062801, 2019.

[27] B.J. Murray, D. O'Sullivan, J.D. Atkinson, and M.E. Webb.
Ice nucleation by particles immersed in supercooled cloud droplets.
Chemical Society Reviews, 41(19):6519 – 6554, 2012.

[28] D. Kashchiev.
Nucleation.
Butterworth-Heinemann, Oxford, page 434, 2000.

[29] L. Lupi, A. Hudait, B. Peters, M. Grünwald, R. Gotchy Mullen, A.H. Nguyen, and V. Molinero.
Role of stacking disorder in ice nucleation.
Nature, 551:218–222, 2017.

[30] A Bogdan.
Thermodynamics of the curvature effect on ice surface tension and nucleation theory.
The Journal of Chemical Physics, 106:1921–1929, 1997.

[31] K. Sudhakar et al.
Design and Applications of Nanostructured Polymer Blends and Nanocomposite Systems.
William Andrew Applied Science Publishers, 2016.

[32] Liu et al.
Determination of supercooling degree, nucleation and growth rates, and particle size for ice slurry crystallization in vacuum.
Crystals, 7(5):128, 2017.

[33] Jörg Stetefeld et al.
Dynamic light scattering: a practical guide and applications in biomedical sciences.
Biophysical Reviews, 8(4):409–427, 2016.

[34] Malvern Instruments Ltd.
Dynamic light scattering: An introduction in 30 minutes.
MRK656-01.

[35] Thomas W. Barlow and A. D. J. Haymet.
Alta: An automated lag-time apparatus for studying the nucleation of supercooled liquids.
Review of Scientific Instruments, 66:2996–3007, 1995.

[36] Yuri G. Gurevich and Jesús Enrique Velázquez-Pérez.
Peltier effect in semiconductors.
Wiley Encyclopedia of Electrical and Electronics Engineering, 2014.

[37] Lei Li, Jesus Rodriguez Sanchez, Felix Kohler, Anja Røyne, and Dag Kristian Dysthe.
Microfluidic control of nucleation and growth of $CaCO_3$.
Crystal Growth and Design, 18(8):4528–4535, 2018.

[38] NASA.
Global Mean Sea Level Trend from Integrated Multi-Mission Ocean Altimeters TOPEX/Poseidon, Jason-1, OSTM/Jason-2, and Jason-3 Version 5.1. Ver. 5.1 PO.DAAC, CA, USA. Dataset accessed [2022-07-21] at https://doi.org/10.5067/GMSLM-TJ151.

[39] D. N. Wiese, D.N Yuan, C. Boening, F. W. Landerer, and M. M. Watkins.
JPL GRACE and GRACE-FO Mascon Ocean, Ice, and Hydrology Equivalent Water Height RL06M CRI Filtered Version 2.0, Ver. 2.0, PO.DAAC, CA, USA, Dataset accessed [2022-07-21] at http://dx.doi.org/10.5067/TEMSC-3MJ62.
pages 409–427, 2019.

[40] S. Olson, M. F. Jansen, D. S. Abbot, I. Halevy, and C. Goldblatt.
The effect of ocean salinity on climate and its implications for earth's habitability.
Geophysical Research Letters, 49(10), 2022.

[41] Jodie Cullum, David P. Stevens, and Manoj M. Joshi.
Importance of ocean salinity for climate and habitability.
PNAS, 113(16):4278–83, 2016.

[42] C.L. Parkinson and D.J. Cavalieri.
Arctic sea ice variability and trends, 1979-2006.
Journal of Geophysical Research, 113(C7), 2008.

[43] Peter Wadhams.
Ice in the Ocean.
CRC Press, 2000.

[44] Linkam Scientific Instruments.
LTS420 and LTS120 User Guide, Ver:1.01.032010.
page 8.

[45] Markus M. Frey et al.
First direct observation of sea salt aerosol production from blowing snow above sea ice.
Atmos. Chem. Phys., 20(4):2549–2578, 2020.

[46] P. A. Alpert, J. Y. Aller, and D. A. Knopf.
Initiation of the ice phase by marine biogenic surfaces in supersaturated gas and supercooled aqueous phases.
Phys. Chem. Chem. Phys., 13(44):19882—19894, 2011.

[47] V. E. Irish, P. Elizondo, J. Chen, C. Chou, J. Charette, M. Lizotte, L. A. Ladino, T. W. Wilson, B. J. Gosselin, M. amd Murray, E. Polishchuk, J. P. D. Abbatt, L. A. Miller, and A. K. Bertram.
Ice-nucleating particles in canadian arctic seasurface microlayer and bulk seawater.
Atmos. Chem. Phys, 17:10583–10595, 2017.

[48] Soleil E. Worthy, Anand Kumar, Yu Xi, Jingwei Yun, Jessie Chen, Cuishan Xu, Victoria E. Irish, Pierre Amato, and Allan K. Bertram.
The effect of $(NH_4)_2SO_4$ on the freezing properties of non-mineral dust ice nucleating substances of atmospheric relevance.
Atmos. Chem. Phys., 21(19):14631–14648, 2021.

[49] Stephen G. Warren, Ignatius G. Rigor, Norbert Untersteiner, Vladimir F. Radionov, Nikolay N. Bryazgin, Yevgeniy I. Aleksandrov, and Roger Colony.
Snow depth on arctic sea ice.

Journal of Climate, 12(6):1814–1829, 1998.

[50] Martin. I. Daily et al.
An evaluation of the heat test for the ice-nucleating ability of minerals and biological material.
Atmos. Meas. Tech, 15(8):2635–2665, 2022.

[51] Hgd homogentisate 1,2-dioxygenase. updated aug 2022, retrieved from `https://www.ncbi.nlm.nih.gov/gene/3081#gene-expression`.
National Center for Biotechnology Information.

[52] J.A. Gallagher, L.R. Ranganath, and A. Zatkova.
Alkaptonuria.
Brenner's Encyclopedia of Genetics, pages 71–75, 2013.

[53] Chanika Phornphutkul et al.
Natural history of alkaptonuria.
N Engl J Med, 347(26):2111–21, 2002.

[54] J.R Stone.
Cardiovascular Pathology (Fourth Edition), Diseases of Small and Medium-sized Blood Vessels.
Academic Press, 2016.

[55] WHO.
Keeping kidneys.
Bull World Health Organization, 90(10):718–719, 2012.

[56] A. Ardehali.
While millions and millions of lives have been saved, organ transplantation still faces massive problems after 50 years; organ preservation is a big part of the solution.
Cryobiology, 71:164–5, 2015.

[57] P.P Reese, M.N Harhay, P.L Abt, M.H Levine, and S.D. Halpern.
New solutions to reduce discard of kidneys donated for transplantation.
J Am Soc Nephrol., 27(4):973–80, 2016.

[58] T.H Jang, S.C Park, J.H Yang, J.Y Kim, J.H Seok, U.S Park, C.W Choi, S.R Lee, and J. Han.
Cryopreservation and its clinical applications.
Integr Med Res, 6(1):12–18, 2017.

[59] D.E. Pegg.
Principles of cryopreservation in cryopreservation and freeze-drying protocols.
Methods in Molecular Biology, Humana Press, 368, 2007.

[60] Harold P. Erickson.
Size and shape of protein molecules at the nanometer level determined by sedimentation, gel filtration, and electron microscopy.
Biological Procedures Online, 11(1):32–51, 2009.

[61] J. Bechhoefer.
Solidification of viscous melts: the interplay of nano- and macroscopic phenomena.
International Journal of Nanotechnology, 5(9-12):1121–1137, 2008.

[62] Past weather in bristol, retrieved from `https://www.timeanddate.com/weather/uk/bristol/historic`.

[63] Robson O. Piucco, Christian J. L. Hermes, Claudio Melo, and Jader R. Barbosa.
A study of frost nucleation on flat surfaces: Theoretical model and experimental validation.
International Refrigeration and Air Conditioning Conference., page 878, 2008.